Measurement of the reaction $K^+n_\uparrow \to K^+\pi^-p$ at 5.98 and 11.85 GeV/c using a transversely polarized deuteron target

A. de Lesquen, L. van Rossum, M. Svec,* M. Babou,† J. Bystricky, G. Cozzika, T. Dobrowolski, Y. Ducros, M. Fujisaki,‡ A. Gaidot, C. F. Hwang,§ A. Itano,** F. Khantine-Langlois, and F. Lehar

Département de Physique des Particules Elémentaires, Centre d'Etudes Nucléaires de Saclay, Gif-sur-Yvette, France

(Received 8 April 1988)

In an experiment carried out at the CERN Proton Synchrotron and using the CERN polarized deuteron target, the reaction $K^+n_\uparrow \to K^+\pi^-p$ was measured in the region $-t=0.1-1.0$ (GeV/c)^2 and $m(K^+\pi^-)=0.812-0.972$ GeV at incident momenta of 5.98 and 11.8 GeV/c. The experiment yields the m and t dependence of 14 linearly independent spin-density-matrix elements describing the coherent production of $K^+\pi^-$ states with dimeson spins $J=0$ and $J=1$. This first measurement of the $KN \to K\pi N$ reaction on a polarized target enables us to study experimentally pion production on the level of production amplitudes. Although the mass dependence of partial cross sections averaged over nucleon spins is smooth, we observe large and systematic structures in the moduli squared of individual nucleon transversity amplitudes which reveal an unexpected but essential role of nucleon spin in the pion production process. Our polarization data suggest the possibility of a new state $I=\frac{1}{2}$ $0^{++}(860)$ with a width of 20–40 MeV. At present we consider this conclusion as only tentative. The predictions of the additive quark model relating $K^+n_\uparrow \to K^{*0}p$ and $p_\uparrow p \to \Delta^{++}n$ are well satisfied at 6 GeV/c. Our results emphasize the need for a systematic study of single-pion production in a new generation of dedicated experiments with spin at the recently proposed high-intensity hadron facilities.

I. INTRODUCTION

This first study of the reaction $K^+n_\uparrow \to K^+\pi^-p$ on transversely polarized quasifree neutrons was carried out at the CERN Proton Synchrotron (PS) using the CERN polarized deuteron target. The experimental apparatus[1] was designed primarily for the measurement of polarization in $K^+n \to K^0p$ (Refs. 2–5) but the data acquisition was triggered also on several other channels with incident kaons[6] and pions[6–9] at $p_{\rm lab}=5.98$ and 11.85 GeV/c. The data for $K^+n \to K^+\pi^-p$ cover the region of four-momentum transfer squared $-t$ from 0.1 to 1.0 (GeV/c)^2 and of the $(K^+\pi^-)$ invariant mass m from 0.812 to 0.972 GeV. In this region the reaction proceeds predominantly by $K^+n \to K^*(892)p$. The data analysis uses 12 000 events at 5.98 GeV/c and 2000 events at 11.85 GeV/c. Preliminary results were published earlier.[10–13] Numerical results are available in the form of tables[14] or can be accessed in the particle data bases at Berkeley or Rutherford Laboratory. Amplitude analysis[14] based on this experiment and its use in new tests of additive quark model[15] will be published elsewhere.

Our experiment adds to the short list of the first-generation measurements of meson production on polarized targets: the Saclay measurement of $\pi^-np \to \pi^+\pi^-$ at 5.98 and 11.85 GeV/c (Ref. 7 and 14); the CERN-Munich-Cracow measurement at 17.2 GeV/c of the reactions $\pi^-p_\uparrow \to \pi^-\pi^+n$ (Refs. 16 and 17), $\pi^-p_\uparrow \to K^-K^+n$,[18] and $\pi^-p_\uparrow \to \pi^-\pi^+\pi^-p$ (Ref. 19); and the Serpukhov measurement of $\pi^-p_\uparrow \to \pi^0\pi^0n$ at 40 GeV/c (Ref. 20). At Argonne, the reaction $p_\uparrow p \to p\pi^+n$ was measured with polarized proton beam momenta ranging from 1.2–2.0 GeV/c (Ref. 21) and 3.0–12.0 GeV/c (Refs. 22 and 23), and the reaction $p_\uparrow p \to p\pi^+\pi^-p$ was studied at 11.75 GeV/c (Ref. 24). Low-energy experiments on $n_\uparrow p \to pp\pi^-$ are in progress at SATURNE II (Saclay) (Ref. 25) and at TRIUMF (Ref. 26). At SLAC, the reaction $\gamma_\uparrow p \to \pi^+\pi^-\pi^0\pi^0p$ was studied at 20 GeV/c using a polarized photon beam.[27]

The previous measurements of $K^+n \to K^+\pi^-p$ on unpolarized targets covered the energy region from 0.7 to 12.0 GeV/c (Refs. 28 and 29). The $K^+\pi^-$ production was found dominated by S- and P-wave $K^+\pi^-$ states for dimeson masses $m(K^+\pi^-) \le 1000$ MeV. These experiments measured, in addition to the cross section $d^2\sigma/(dm\,dt)$, five unpolarized spin-density-matrix (SDM) elements as a function of invariant mass m and momentum transfer squared t. Comparisons with the line reversed reaction $K^-p \to K^-\pi^+n$ revealed violation of exchange degeneracy for isovector exchanges.[29]

Extrapolations of the $KN \to K\pi N$ data into the unphysical region of t were used to perform phase-shift analyses of $K\pi \to K\pi$ reactions[29,30] extending to other channels similar work on $\pi\pi \to \pi\pi$ (Refs. 31–34). These studies relied on several necessary technical assumptions. Since only the s-channel unnatural-exchange nucleon-helicity-flip amplitudes should be extrapolated to the pion pole, a crucial assumption required that either all unnatural-exchange s-channel nucleon-helicity-nonflip amplitudes vanish,[30–34]

$$n_i = 0 \ , \tag{1.1}$$

or each unnatural-exchange s-channel nucleon-helicity-nonflip amplitude is directly proportional to the associated flip amplitude:[35]

$$n_i = c f_i \ , \tag{1.2}$$

where $c = c(m,t)$ is a common function of m and t. Both assumptions lead to simple predictions for the spin-dependent observables which measure the interference between the nucleon-helicity-nonflip and -flip amplitudes. These predictions are testable in experiments with transversely polarized targets.

Our experiment confirms the S- and P-wave dominance of the $K^+\pi^-$ production for $m(K^+\pi^-) \leq 950$ MeV and measures 14 SDM elements in both s- and t-channel helicity frames. The results for five unpolarized SDM elements agree with the previous measurements.[29] The nine new spin-dependent observables reveal evidence for nontrivial nucleon helicity nonflip amplitudes ("A_1-Z" exchange). This observation is in agreement with measurements of $\pi N \to \pi^+\pi^- N$ on polarized targets which also observe nontrivial helicity-nonflip amplitudes and A_1-exchange signal.[7,16] Our data contradict the predictions for polarized SDM elements based on the assumptions (1.1) and (1.2) used previously in the studies of meson-meson scattering. The measured polarized SDM elements provide the first experimental information on pion production by kaons on the level of production amplitudes. The results reveal the important and complex role of nucleon spin in the pion production process.

Our paper is organized in six sections. The kinematics, observables, and amplitudes are introduced in Sec. II with a short overview of some of their properties. The experiment and data analysis are described in Secs. III and IV, respectively. Our results are described and discussed in Sec. V. Section VI closes the paper with a summary of results and a discussion of the outlook for a new generation of experiments with spin at the recently proposed high-intensity hadron facilities. The Appendix describes the conventions used in the definition of nucleon transversity amplitudes.

II. KINEMATICS, OBSERVABLES, AND AMPLITUDES

A. Kinematics

The kinematical variables used to describe the dimeson production on a polarized nucleon target at rest are $(s,t,m,\theta,\varphi,\psi,\delta)$ (Refs. 36 and 37) where s is the c.m.-system (c.m.s) energy squared, t is the four-momentum transfer squared, and m is the $K^+\pi^-$ invariant mass. The angles (φ,θ) describe the direction of the K^+ in the $K^+\pi^-$ rest frame. The angles (ψ,δ) describe the direction of target nucleon polarization in the target nucleon rest frame. The angle ψ is the angle between the direction of target transverse polarization and the normal to the production plane (Fig. 1). Our analysis is carried out in both the s- and the t-channel helicity frames for the $K^+\pi^-$ dimeson system. The helicities of the initial and final nucleons are always defined in the s-channel helicity frame.

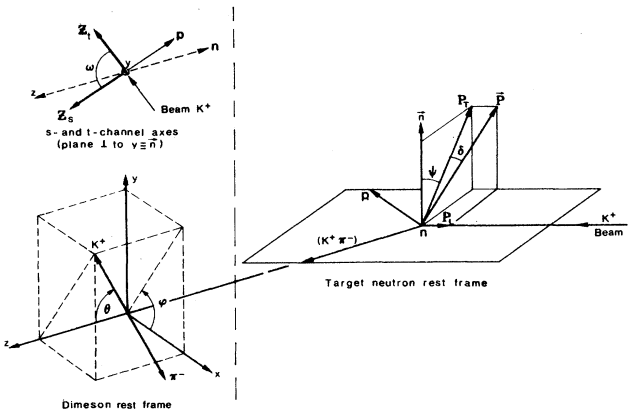

FIG. 1. Definition of the coordinate systems used to describe the target polarization **P** and the decay of the dimeson $K^+\pi^-$ system.

B. Observables

When the polarization of the recoil nucleon is not observed, the angular distribution $I(\theta,\varphi,\psi,\delta)$ of $K^+\pi^-$ production on polarized nucleons at rest can be expressed in terms of the normalized distribution $W(\theta,\varphi,\psi,\delta)$:

$$I(\theta,\varphi,\psi,\delta) = W(\theta,\varphi,\psi,\delta) d^2\sigma/(dt\,dm) \ , \tag{2.1}$$

where

$$\frac{d^2\sigma}{(dt\,dm)} = \int I(\theta,\varphi,\psi,\delta) d\Omega\, d\psi\, d(-\sin\delta) \tag{2.2}$$

is the $K^+\pi^-$ production cross section at fixed values of s, t, and m. The distribution $W(\theta,\varphi,\psi,\delta)$ can be written[38–43] as a sum of four terms:

$$W(\theta,\varphi,\psi,\delta) = W_0(\theta,\varphi) + P_T \cos\psi\, W_y(\theta,\varphi) + P_T \sin\psi\, W_x(\theta,\varphi) + P_L W_z(\theta,\varphi) \ , \tag{2.3}$$

where $P_T = P\cos\delta$ and $P_L = P\sin\delta$ are the transverse and longitudinal components of target polarization **P** with respect to the incident momentum (Fig. 1). The simple $\cos\psi$,$\cos\delta$,$\sin\delta$ dependence is due to spin $\frac{1}{2}$ of the target nucleon.[41,43] Parity conservation requires that W_0 and W_y (W_x and W_z) be symmetric (antisymmetric) in φ (Refs. 38 and 43).

In the data analysis of $K^+\pi^-$ angular distribution, it is convenient to use expansions of the angular distribution into spherical harmonics.[39–44] In the usual notation

$$W_0(\Omega) = \sum_{L,M} t_M^L \mathrm{Re} Y_M^L(\Omega) \ ,$$
$$W_y(\Omega) = \sum_{L,M} p_M^L \mathrm{Re} Y_M^L(\Omega) \ , \tag{2.4}$$
$$W_x(\Omega) = \sum_{L,M} r_M^L \mathrm{Im} Y_M^L(\Omega), \quad W_z(\Omega) = \sum_{L,M} q_M^L \mathrm{Im} Y_M^L(\Omega) \ .$$

The expansion coefficients t,p,r,q are called multipole parameters. They are simply related to the momenta of angular distribution:[39,41,43]

$$
\begin{aligned}
t_M^L &= \epsilon_M \langle \mathrm{Re}\, Y_M^L \rangle \\
&= \frac{\epsilon_M}{2\pi} \int I(\Omega,\psi,\delta)\mathrm{Re}\, Y_M^L(\Omega)\, d\Omega' , \\
p_M^L &= 2\epsilon_M \langle \cos\delta \cos\psi\, \mathrm{Re}\, Y_M^L \rangle \\
&= \frac{2\epsilon_M}{2\pi} \int I(\Omega,\psi,\delta)\mathrm{Re}\, Y_M^L(\Omega)\cos\delta\cos\psi\, d\Omega' , \\
r_M^L &= 4\langle \cos\delta \sin\psi\, \mathrm{Im}\, Y_M^L \rangle \\
&= \frac{4}{2\pi} \int I(\Omega,\psi,\delta)\mathrm{Im}\, Y_M^L(\Omega)\cos\delta\sin\psi d\Omega' , \\
q_M^L &= 4\langle \sin\delta\, \mathrm{Im}\, Y_M^L \rangle \\
&= \frac{4}{2\pi} \int I(\Omega,\psi,\delta)\mathrm{Im}\, Y_M^L(\Omega)\sin\delta d\Omega' ,
\end{aligned}
\tag{2.5}
$$

where $d\Omega' = d\Omega\, d\psi d(-\sin\delta)$. In (2.5), $\epsilon_M = 1$ for $M=0$ and $\epsilon_M = 2$ for $M \neq 0$. Integrated over the solid angles (θ,φ), the distribution (2.1) becomes

$$
I(\psi,\delta) = (1 + AP_T\cos\psi)\frac{d^2\sigma}{dm\, dt} , \tag{2.6}
$$

where $A = A(s,t,m) = (4\pi)^{1/2}p_0^0$ is the polarized-target asymmetry analogous to the polarization parameter measured in two-body reactions.

The utility of angular expansions (2.4) in data analyses of pion production is based on the assumption that the truncation of the series at some $L = L_{\max}$ is uniformly good for all solid angles $\Omega = (\theta,\varphi)$ at given values of s, m, and t. In practice, a stronger assumption is often used: the truncation is uniformly good also for all s and t at given value of m. In this case $L_{\max}$ is a step function of m only.

The $K^+\pi^-$ system is not produced, in general, in a state of definite spin and parity. The polarization of the $K^+\pi^-$ system is described by spin-density matrix with complex matrix elements $\rho_{\lambda\lambda'}^{JJ'}$, where J,J' and λ,λ' are the dimeson spins and helicities, respectively.[38–43] Omitting the indices J,J',λ,λ' for clarity, the SDM elements $\rho_{\lambda\lambda'}^{JJ'}$ for the $K^+\pi^-$ production on polarized target have a general form[26–29]

$$
\rho = \rho^0 + P_T\cos\psi\rho^y + P_T\sin\psi\rho^x + P_L\rho^z . \tag{2.7}
$$

The components of angular distribution, $W_k(\theta,\varphi), k = 0,y,x,z$, can be expressed in terms of the matrix elements of the corresponding component ρ^k of the SDM elements[42,43]

$$
W_k(\Omega) = \sum_{J,\lambda}\sum_{J',\lambda'} \rho_{\lambda\lambda'}^{k,JJ'} Y_\lambda^J(\Omega) Y_{\lambda'}^{J'*}(\Omega) . \tag{2.8}
$$

Using the Hermiticity of SDM elements, parity conservation, and properties of spherical harmonics, the multipole parameters (2.5) can be related to the SDM elements (2.7). For the parameters t_M^L we have[41,43]

$$
t_M^L = \sum_{J,\lambda}\sum_{J',\lambda'} \begin{pmatrix} L & J & J' \\ M & \lambda & \lambda' \end{pmatrix} \mathrm{Re}(\rho_{\lambda\lambda'}^{0,JJ'}) , \tag{2.9}
$$

where the summing is constrained by

$$
|J-J'| \le L \le J+J', \quad M = \lambda - \lambda' \tag{2.10a}
$$

and the symbol

$$
\begin{aligned}
\begin{pmatrix} L & J & J' \\ M & \lambda & \lambda' \end{pmatrix} &= (-1)^{\lambda'} \left[\frac{(2J+1)(2J'+1)^{1/2}}{4\pi(2L+1)} \right]^{1/2} \\
&\times \langle JJ'00|L0\rangle \langle JJ'\lambda\lambda'|LM\rangle .
\end{aligned}
\tag{2.10b}
$$

Analogous relations hold between p_M^L, r_M^L, q_M^L and the SDM elements $\mathrm{Re}(\rho_{\lambda\lambda'}^{y,JJ'})$, $\mathrm{Im}(\rho_{\lambda\lambda'}^{x,JJ'})$, $\mathrm{Im}(\rho_{\lambda\lambda'}^{z,JJ'})$, respectively. Assuming parity conservation, the SDM elements $\mathrm{Im}(\rho^0)$, $\mathrm{Im}(\rho^y)$, $\mathrm{Re}(\rho^x)$, $\mathrm{Re}(\rho^z)$, are not directly observable in experiments which do not measure recoil nucleon polarization.

When the $K^+\pi^-$ dimeson system is produced only in the spin states with $J=0$ (S wave) and $J=1$ (P wave), the relations between the multipole parameters and the observable SDM elements become particularly simple. For clarity we will omit the superscripts JJ' and the superscript $k=0$. The relations for t_M^L and r_M^L read

$$
\begin{aligned}
&t_0^0 = K(\rho_{ss} + \rho_{00} + 2\rho_{11}), \quad t_0^1 = 2K\, \mathrm{Re}\rho_{0s} , \\
&t_0^2 = (\tfrac{4}{5})^{1/2}K(\rho_{00} - \rho_{11}), \quad t_1^1 = 4K\, \mathrm{Re}\rho_{1s} , \\
&t_1^2 = (\tfrac{48}{5})^{1/2}K\, \mathrm{Re}\rho_{10}, \quad t_2^2 = -(\tfrac{24}{5})^{1/2}K\rho_{1-1} ,
\end{aligned}
\tag{2.11}
$$

$$
\begin{aligned}
&r_1^1 = -\sqrt{32}K\, \mathrm{Im}\rho_{1s}^x , \\
&r_1^2 = (\tfrac{24}{5})^{1/2}K\, \mathrm{Im}\rho_{10}^x , \\
&r_2^2 = +(\tfrac{24}{5})^{1/2}K\, \mathrm{Im}\rho_{1-1}^x ,
\end{aligned}
\tag{2.12}
$$

where $K = 1/(4\pi)^{1/2}$. The helicity λ of the $K^+\pi^-$ system is $\lambda = s$ and $\lambda = -1,0,+1$ for S wave and P wave, respectively. The relations for the p_M^L and q_M^L in terms of the SDM elements $\mathrm{Re}(\rho_{\lambda\lambda'}^{y,JJ'})$ and $\mathrm{Im}(\rho_{\lambda\lambda'}^{z,JJ'})$ are analogous to the Eqs. (2.11) and (2.12), respectively.

When the $K^+\pi^-$ system is produced also in spin states with $J \ge 2$, the relations between multipole parameters and SDM elements become an undetermined set of linear equations for SDM elements. Explicit formulas for t_M^L are given in Ref. 45 up to $J=2$ (D wave) and in Ref. 46 up to $J=3$ (F wave). Positivity and rank conditions,[47–53] and nonlinear relations of La France-Winternitz type[54] provide additional constraints on SDM elements. A possible general method of solving the equations for SDM elements is discussed in Ref. 53.

This experiment does not measure $W_z(\Omega)$ since the longitudinal component of polarization $P_L = 0$. The Fermi motion of the target neutron in the laboratory system introduces only a small correction to the effective neutron polarization (Sec. III). Assuming S- and P-wave dominance, the explicit form of the K^+ angular distribution in terms of the $K^+\pi^-$ SDM elements reads

$$
\begin{aligned}
4\pi W(\theta,\varphi,\psi)|_{s,t,m} = &\{(\rho_{ss}+\rho_{00}+2\rho_{11})+(\rho_{00}-\rho_{1-1})[3\cos^2(\theta)-1]-\rho_{1-1}3\sin^2(\theta)\cos(2\varphi)\\
&-\mathrm{Re}\rho_{10}3\sqrt{2}\sin(2\theta)\cos(\varphi)+\mathrm{Re}\rho_{0s}2\sqrt{3}\cos(\theta)-\mathrm{Re}\rho_{1s}2\sqrt{6}\sin(\theta)\cos(\varphi)\}\\
&+P_T\cos\psi\{(\rho^y_{ss}+\rho^y_{00}+2\rho^y_{11})+(\rho^y_{00}-\rho^y_{1-1})[3\cos^2(\theta)-1]\\
&-\rho^y_{1-1}3\sin^2(\theta)\cos(2\varphi)-\mathrm{Re}\rho^y_{10}3\sqrt{2}\sin(2\theta)\cos(\varphi)\\
&+\mathrm{Re}\rho^y_{0s}2\sqrt{3}\cos(\theta)-\mathrm{Re}\rho^y_{1s}2\sqrt{6}\sin(\theta)\cos(\varphi)\}\\
&+P_T\sin\psi[\mathrm{Im}\rho^x_{1-1}3\sin^2(\theta)\sin(2\varphi)+\mathrm{Im}\rho^x_{10}3\sqrt{2}\sin(2\theta)\sin(\varphi)\\
&+\mathrm{Im}\rho^x_{1s}2\sqrt{6}\sin(\theta)\sin(\varphi)] \ . \qquad (2.13)
\end{aligned}
$$

There are two linear relations among the matrix elements in (2.13):

$$\rho_{ss}=\rho_{00}+2\rho_{11}=1 \ , \qquad (2.14a)$$

$$\rho^y_{ss}+\rho^y_{00}+2\rho^y_{11}=A \ , \qquad (2.14b)$$

where A is the polarized target asymmetry.

For reasons of brevity we shall write the expression (2.13) in a simplified form

$$4\pi W(\theta,\varphi,\psi)=1+\sum_{i=2}^{15} a_i C_i(\psi) Y_i(\theta,\varphi) \ , \qquad (2.15)$$

where the coefficients

$$C_i=\begin{cases} 1 \ \text{ for } i=2,\ldots,6 \ , \\ P_T\cos\psi \ \text{ for } i=7,\ldots,12 \ , \\ P_T\sin\psi \ \text{ for } i=13,14,15 \ . \end{cases}$$

The parameters a_i, $i=2,\ldots,15$ are the combinations of normalized spin-density-matrix elements in Eq. (2.13) that are to be determined by the experiment.

C. Amplitudes

The reaction $K^+n\to K^+\pi^-p$ is described by production amplitudes $H_{\lambda_p,0\lambda_n}(s,t,m,\theta,\varphi)$ where λ_p and λ_n are the helicities of the proton and neutron, respectively. The production amplitudes can be expressed in terms of production amplitudes corresponding to definite dimeson spin J using an angular expansion

$$H_{\lambda_p,0\lambda_n}=\sum_{J=0}^{\infty}\sum_{\lambda=-J}^{+J}(2J+1)^{1/2}H^J_{\lambda\lambda_p,0\lambda_n}(s,t,m)\times d^J_{\lambda 0}(\theta)e^{i\lambda\varphi} \ , \qquad (2.16)$$

where J is the spin and λ the helicity of the $(K^+\pi^-)$ dimeson system. The "partial-wave" amplitudes $H^J_{\lambda\lambda_p,0\lambda_n}$ can be expressed in terms of nucleon helicity amplitudes with definite t-channel-exchange naturality. The nucleon s-channel helicity amplitudes describing the production of the $(K^+\pi^-)$ system in the S- and P-wave states are

$$
\begin{aligned}
0^-\tfrac{1}{2}^+\to 0^+\tfrac{1}{2}^+ &: \ H^0_{0+,0+}=S_0 \ , \\
&\quad\ H^+_{0+,0-}=S_1 \ ; \\
0^-\tfrac{1}{2}^+\to 1^-\tfrac{1}{2}^+ &: \ H^1_{0+,0+}=L_0 \ , \\
&\quad\ H^1_{0+,0-}=L_1 \ , \\
&\quad\ H^1_{\pm 1+,0+}=\frac{N_0\pm U_0}{\sqrt{2}} \ , \\
&\quad\ H^1_{\pm 1+,0-}=\frac{N_1\pm U_1}{\sqrt{2}} \ .
\end{aligned} \qquad (2.17)
$$

At large s, the amplitude N_0 and N_1 are dominated by natural exchanges "A_2-ρ." The amplitudes S_n, L_n, U_n, $n=0,1$ are dominated by unnatural exchanges: "A_1-Z" for $n=0$ and "π-B" for $n=1$. The "Z" and "B" are isovector $J^{PC}=2^{--}$ and 1^{+-} t-channel exchanges, respectively. The index $n=|\lambda_n-\lambda_p|$ is nucleon helicity flip.

The observables obtained in experiments on transversely polarized nucleon target in which recoil nucleon polarization is not observed are most simply related to nucleon transversity amplitudes (NTA) of definite naturality. For the S and P waves they are defined as

$$
\begin{aligned}
S&=\frac{S_0+iS_1}{\sqrt{2}}, \quad \bar{S}=\frac{S_0-iS_1}{\sqrt{2}} \ , \\
L&=\frac{L_0+iL_1}{\sqrt{2}}, \quad \bar{L}=\frac{L_0-iL_1}{\sqrt{2}} \ , \\
U&=\frac{U_0+iU_1}{\sqrt{2}}, \quad \bar{U}=\frac{U_0-iU_1}{\sqrt{2}} \ , \\
N&=\frac{N_0-iN_1}{\sqrt{2}}, \quad \bar{N}=\frac{N_0+iN_1}{\sqrt{2}} \ .
\end{aligned} \qquad (2.18)
$$

In this case the measured observables form a closed set of equations which allow a determination of moduli of NTA and cosines of certain relative phases.[14,16,41,42]

The nucleon helicity and transversity amplitudes differ in the quantization axis for the nucleon spin.[55,56] The transversity amplitudes S,L,U,N $(\bar{S},\bar{L},\bar{U},\bar{N})$ describe production of the dimeson state with the recoil nucleon spin antiparallel or "down" (parallel or "up") to the normal **n** of the production plane (defined by the Basel convention). Using the symbols $\uparrow$ and $\downarrow$ for the nucleon transversities up and down, respectively, the following table shows the spin states of target neutrons and recoil

protons and the dimeson helicities corresponding to the transversity amplitudes (2.18):

	n	p	$(K^+\pi^-)$
S,L	↑	↓	0
$\bar{S},\bar{L}$	↓	↑	0
U	↑	↓	+1 or −1
$\bar{U}$	↓	↑	+1 or −1
N	↓	↓	+1 or −1
$\bar{N}$	↑	↑	+1 or −1

(2.19)

Parity conservation requires that in the transversity frame the dimeson production with helicities $\lambda=\pm1$ depends only on the transversities of the initial and final nucleons. The amplitudes $U,\bar{U},N,\bar{N}$ do not distinguish between the dimeson helicity states with $\lambda=+1$ or -1. Also, the dimeson production with helicity $\lambda=0$ is forbidden by parity conservation when the initial and final nucleons have the same transversities.

Our convention for transversity amplitudes is discussed in the Appendix.

D. Observables in terms of amplitudes

To interpret the experimental results it is instructive to express the measured observables in terms of both nucleon helicity and recoil nucleon transversity amplitudes. In our normalization, the integrated cross section (2.2) is

$$\frac{d^2\sigma}{dm\,dt}=|S|^2+|\bar{S}|^2+|L|^2+|\bar{L}|^2+|U|^2+|\bar{U}|^2 +|N|^2+|\bar{N}|^2 . \tag{2.20}$$

With $\Sigma\equiv d^2\sigma/dm\,dt$, the relations for SDM elements in terms of helicity amplitudes read as follows.

Unpolarized SDM elements:

$$\begin{aligned}
&(\rho_{ss}+\rho_{00}+2\rho_{11})\Sigma=\sum_{n=0,1}|S_n|^2+|L_n|^2+|U_n|^2+|N_n|^2 ,\\
&(\rho_{00}-\rho_{11})\Sigma=\sum_{n=0,1}|L_n|^2-\tfrac{1}{2}(|N_n|^2+|U_n|^2) ,\\
&\rho_{1-1}\Sigma=\sum_{n=0,1}\tfrac{1}{2}(|N_n|^2-|U_n|^2) ,\\
&\sqrt{2}\,\mathrm{Re}\rho_{10}\Sigma=\sum_{n=0,1}\mathrm{Re}(U_nL_n^*) ,\\
&\sqrt{2}\,\mathrm{Re}\rho_{1s}\Sigma=\sum_{n=0,1}\mathrm{Re}(U_nS_n^*) ,\\
&\mathrm{Re}\rho_{0s}\Sigma=\sum_{n=0,1}\mathrm{Re}(L_nS_n^*) .
\end{aligned} \tag{2.21a}$$

Polarized SDM elements:

$$\begin{aligned}
&(\rho^y_{ss}+\rho^y_{00}+2\rho^y_{11})\Sigma=2\,\mathrm{Im}(S_0S_1^*+L_0L_1^*+U_0U_1^*+N_0N_1^*),\\
&(\rho^y_{00}-\rho^y_{11})\Sigma=\mathrm{Im}(2L_0L_1^*-N_0N_1^*-U_0U_1^*) ,\\
&\rho^y_{1-1}\Sigma=\mathrm{Im}(N_0N_1^*-U_0U_1^*) ,\\
&\sqrt{2}\,\mathrm{Re}\rho^y_{10}\Sigma=\mathrm{Im}(U_0L_1^*-U_1L_0^*) ,\\
&\sqrt{2}\,\mathrm{Re}\rho^y_{1s}\Sigma=\mathrm{Im}(U_0S_1^*-U_1S_0^*) ,\\
&\mathrm{Re}\rho^y_{0s}\Sigma=\mathrm{Im}(L_0S_1^*-L_1S_0^*) ,
\end{aligned} \tag{2.21b}$$

$$\begin{aligned}
&-\mathrm{Im}\rho^x_{1-1}\Sigma=\mathrm{Im}(N_0U_1^*+N_1U_0^*) ,\\
&\sqrt{2}\,\mathrm{Im}\rho^x_{10}\Sigma=\mathrm{Im}(N_0L_1^*+N_1L_0^*) ,\\
&\sqrt{2}\,\mathrm{Im}\rho^x_{1s}\Sigma=\mathrm{Im}(N_0S_1^*+N_1S_0^*) .
\end{aligned} \tag{2.21c}$$

Only the polarization-dependent SDM elements measure the nucleon helicity-flip-nonflip interference. The observables (2.21b) and (2.21c) measure the interference between the amplitudes of the same and opposite naturalities, respectively.

To express the observables in terms of transversity amplitudes, it is convenient to work with the sum and the difference of SDM elements (2.21a) and (2.21b). Using the notation of (2.14), the relations for the sums read

$$\begin{aligned}
&\tfrac{1}{2}(1+A)\Sigma=|S|^2+|L|^2+|U|^2+|\bar{N}|^2 ,\\
&\tfrac{1}{2}[(\rho_{00}-\rho_{11})+(\rho^y_{00}-\rho^y_{11})]\Sigma=2|L|^2-|U|^2-|\bar{N}|^2 ,
\end{aligned} \tag{2.22a}$$

$$\begin{aligned}
&\tfrac{1}{2}(\rho_{1-1}+\rho^y_{1-1})\Sigma=|\bar{N}|^2-|U|^2 ,\\
&\frac{1}{\sqrt{2}}(\mathrm{Re}\rho_{10}+\mathrm{Re}\rho^y_{10})\Sigma=\mathrm{Re}(UL^*)\\
&\qquad=|U||L|\cos(\gamma_{UL}) ,\\
&\frac{1}{\sqrt{2}}(\mathrm{Re}\rho_{1s}+\mathrm{Re}\rho^y_{1s})\Sigma=\mathrm{Re}(US^*)\\
&\qquad=|U||S|\cos(\gamma_{US}) ,\\
&\tfrac{1}{2}(\mathrm{Re}\rho_{0s}+\mathrm{Re}\rho^y_{0s})\Sigma=\mathrm{Re}(LS^*)\\
&\qquad=|L||S|\cos(\gamma_{LS}) .
\end{aligned} \tag{2.22b}$$

Similar equations relate the differences of the observables to amplitudes of opposite transversity. For SDM elements (2.21c) we have

$$\begin{aligned}
&-\mathrm{Im}\rho^x_{1-1}\Sigma=\mathrm{Re}(NU^*-\bar{N}\bar{U}^*) ,\\
&\sqrt{2}\,\mathrm{Im}\rho^x_{10}\Sigma=\mathrm{Re}(NL^*-\bar{N}\bar{L}^*) ,\\
&\sqrt{2}\,\mathrm{Im}\rho^x_{1s}\Sigma=\mathrm{Re}(NS^*-\bar{N}\bar{S}^*) .
\end{aligned} \tag{2.22c}$$

The above equations (2.22b) and similar equations for the differences provide information on cosines of relative phases $\cos\gamma$ and $\cos\bar{\gamma}$. Together with the equations (2.22a) they enable a model-independent amplitude analysis.[14]

In our experiment we have not measured $d^2\sigma/(dm\,dt)$. Consequently, we work with normalized amplitudes corresponding to $d^2\sigma/(dm\,dt)\equiv1$.

E. Helicity-frame rotation

In our experiment the nucleon helicities are defined in the s-channel frame while the helicity of the $K^+\pi^-$ system is defined either in the s- or the t-channel frame. The rotation between the two coordinate systems gives

$$S_n^{(t)}=S_n^{(s)},\quad N_n^{(t)}=N_n^{(s)}\ , \tag{2.23a}$$

$$\begin{aligned} L_n^{(t)}&=\cos\chi L_n^{(s)}+\sin\chi U_n^{(s)}\ ,\\ U_n^{(t)}&=-\sin\chi L_n^{(s)}+\cos\chi U_n^{(s)}\ , \end{aligned} \tag{2.24a}$$

when $n=0,1$ and χ is the rotation (crossing) angle.[40,56] For transversity amplitudes we get

$$S^{(t)}=S^{(s)},\quad N^{(t)}=N^{(s)}\ , \tag{2.23b}$$

$$\begin{aligned} L^{(t)}&=\cos\chi\, L^{(s)}+\sin\chi\, U^{(s)}\ ,\\ U^{(t)}&=-\sin\chi\, L^{(s)}+\cos\chi\, U^{(s)}\ , \end{aligned} \tag{2.24b}$$

and similar relations for opposite transversity. The rotation (2.23) leaves invariant the combinations

$$\begin{aligned} &|L_n|^2+|U_n|^2,\quad n=0,1\\ &|L|^2+|U|^2,\quad |\bar{L}|^2+|\bar{U}|^2\ . \end{aligned} \tag{2.25}$$

Data analysis can be tested for self-consistency by examining either the rotated SDM elements, or the helicity frame invariants expressed directly in terms of the measured SDM elements. The frame invariants appear to be more suitable tests.

Equations (2.23) and (2.24) lead to linear frame invariants

$$I_1=\rho_{ss}+\rho_{00}+2\rho_{11}=1\ ,$$

$$I_1^y=\rho_{ss}^y+\rho_{00}^y+2\rho_{11}^y=A\ , \tag{2.26a}$$

$$\begin{aligned} I_2&=\tfrac{1}{3}[1-(\rho_{00}-\rho_{11})]+\rho_{1-1}\ ,\\ I_2^y&=\tfrac{1}{3}[A-(\rho_{00}^y-\rho_{11}^y)]+\rho_{1-1}^y\ , \end{aligned} \tag{2.26b}$$

$$\begin{aligned} I_3&=\tfrac{2}{3}+\tfrac{1}{3}(\rho_{00}-\rho_{11})-\rho_{1-1}=1-I_1\ ,\\ I_3^y&=\tfrac{2}{3}A+\tfrac{1}{3}(\rho_{00}^y-\rho_{11}^y)-\rho_{1-1}^y=A-I_1^y\ , \end{aligned} \tag{2.26c}$$

$$I_4=\mathrm{Im}\rho_{1s}^y\ . \tag{2.26d}$$

The rotation between SDM elements leaves unchanged quadratic invariants

$$\begin{aligned} I_5&=[(\rho_{00}-\rho_{11})+\rho_{1-1}]^2+(2\sqrt{2}\,\mathrm{Re}\rho_{10})^2\ ,\\ I_5^y&=[(\rho_{00}^y-\rho_{11}^y)+\rho_{1-1}^y]^2+(2\sqrt{2}\,\mathrm{Re}\rho_{10}^y)^2 \end{aligned} \tag{2.26e}$$

and linear invariants

$$I_6=\mathrm{Im}\rho_{10},\quad I_6^y=\mathrm{Im}\rho_{10}^y\ . \tag{2.26f}$$

Notice that $\mathrm{Re}\rho_{10}$ enters only in the quadratic invariants. The invariants (2.25f) are useful when violations of P parity are tested.

III. THE EXPERIMENT

The experiment was carried out at the CERN Proton Synchrotron. The CERN polarized-target group had achieved more than 40% deuteron polarization in deuterated propanediol.[57] This development opened the possibility to study interactions on polarized neutrons. We have used this frozen spin target to measure several interactions with nucleon charge exchange, with incident kaon[2-6] and pion[6-9] beams at $p_{\mathrm{lab}}=5.98$ and 11.85 GeV/c.

The lay out of the apparatus at 5.98 GeV/c is shown in Fig. 2. The beam, target, detectors, trigger logic, and electronics are described in detail in Ref. 1. The data acquisition, event reconstruction and selection, and the acceptance calculation are fully described in Ref. 7. The incident K^+ intensity at 5.98 GeV/c (11.85 GeV/c) was about 3.5×10^4 (2.2×10^4) particles per burst representing 2.7% (1.7%) of the total beam intensity. Three gas Cherenkov threshold counters were used for beam parti-

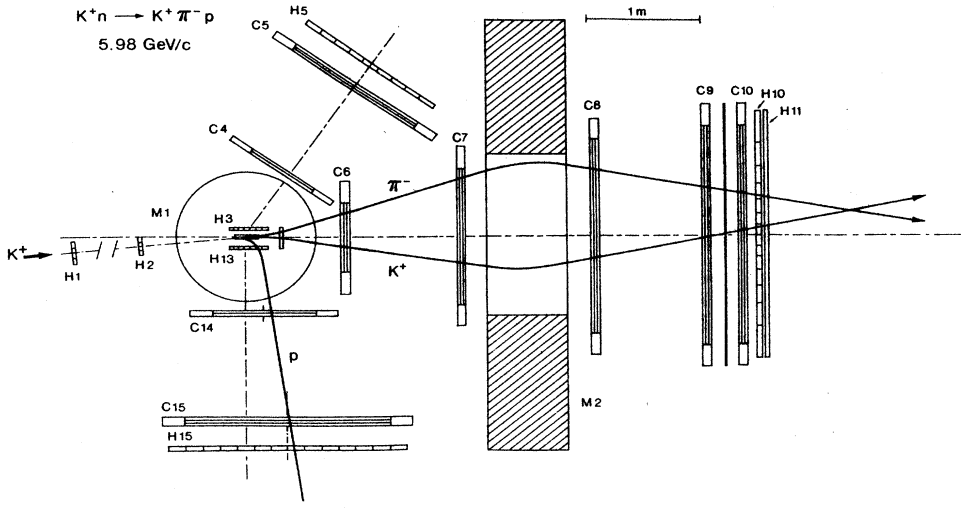

FIG. 2. The layout of the experiment at 5.98 GeV/c. $H_1,\ldots,H_{15}$ are triggering hodoscopes; $C_1,\ldots,C_{15}$ are multiwire proportional chambers; M_1 and M_2 are the target and spectrometer magnets, respectively.

cle identification. The $K^+\pi^-$ pair was detected in the forward spectrometer, and the proton in one of the recoil arms (Fig. 2). The measurement of angle and momentum of the recoil proton is important not only for event reconstruction and selection but also for calculating the effective neutron target polarization. The Fermi momentum of the target neutron was reconstructed using a one-constraint fit. No particle identification was used on the outgoing particles. The fit with hypothesis $K^+n \to K^+\pi^-p$ was sufficient to suppress events with wrong mass assignment. The experimental resolution in t and m was approximately $\Delta t = \pm 0.015$ (GeV/c)^2 and $\Delta m = 10$ MeV.

The event reconstruction and selection resulted in 12 000 events at 5.98 GeV/c and 2000 events at 11.85 GeV/c. This ratio reflects mainly the energy dependence of the $K^+\pi^-$ production cross section. Figure 3 shows the mass and t dependence of the observed number of events. The figure shows that at both energies the reaction proceeds predominantly via $K^+n \to K^{0*}(892)p$. The Dalitz plot of $m(K^+\pi^-)$ vs $m(\pi^-p)$ reveals only a negligible $\Delta^\circ(1236)$ signal.

The effective neutron target polarization is obtained from the deuteron polarization by taking into account (1) the Fermi motion of neutrons and the D-state component of the deuteron wave function, and (2) the probability that the event belongs to the unpolarized background. In the neutron rest frame of each event α we calculate the effective magnitude of the transverse target polarization $P_T^{\text{eff}}(\alpha)$. The longitudinal polarization $P_L^{\text{eff}}(\alpha)$ is found to be too small to be useful for determination of longitudinal SDM elements. The method is described in detail in Ref. 7.

The acceptance in four-momentum transfer squared t covered the region $-t = 0.1-1.5$ (GeV/c)^2 at both energies. The lower limit corresponds to the minimum energy for the proton to be detected and measured. The upper limit results from the aperture of the forward spectrometer. The cross section and acceptance limits the analysis to $-t = 0.1-1.0$ (GeV/c)^2 [Fig. 4(a)]. The acceptance in the dimeson invariant mass ranged from threshold to 1500 MeV with sufficient statistics up to 975 MeV [Fig. 4(b)]. The distribution in the angle ψ was limited to $\Delta\psi = \pm 30^\circ$ around $\psi = 0$ and π by the acceptance of the recoil arms. Consequently, the observables depending on the transverse component of target polarization in the production plane are obtained with less precision. The calculation of acceptance is described in Ref. 7.

The estimate of acceptance corrected cross sections is

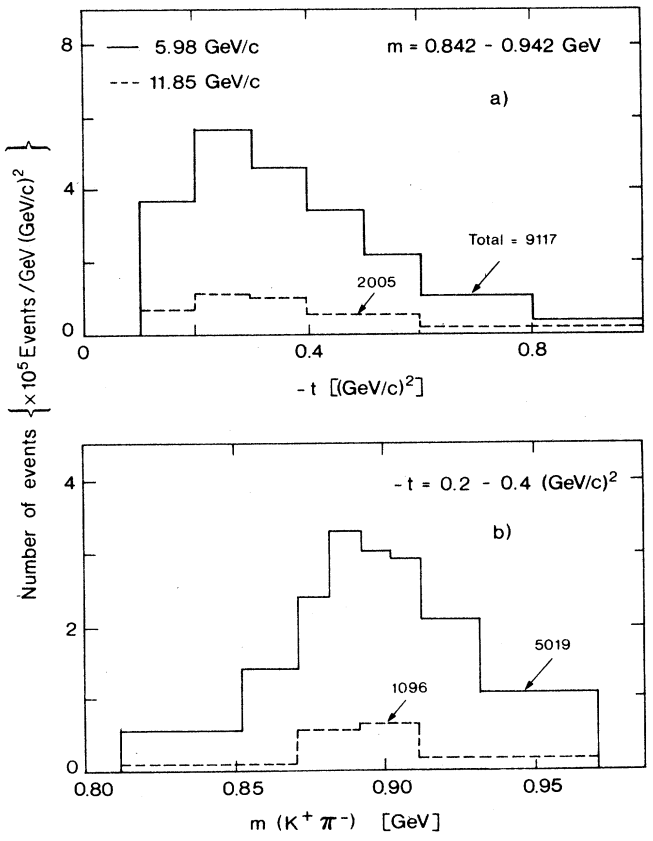

FIG. 3. The raw $K^+\pi^-$ mass spectra at 5.98 (solid) and 11.85 GeV/c (dashed) uncorrected for acceptance. (a) The t dependence for dimeson mass interval $m = 842-942$ MeV. (b) The m dependence for the interval of four-momentum transfer squared $-t = 0.2-0.4$ (GeV/c)^2.

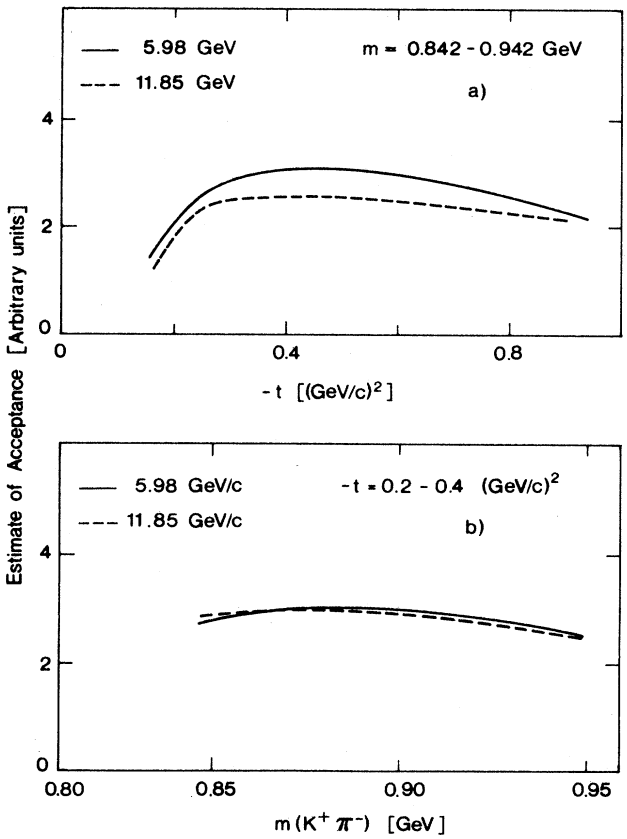

FIG. 4. The t dependence (a) and the mass dependence (b) of geometrical acceptance integrated over the true angular distribution in θ, φ, and ψ at 5.98 and 11.85 GeV/c.

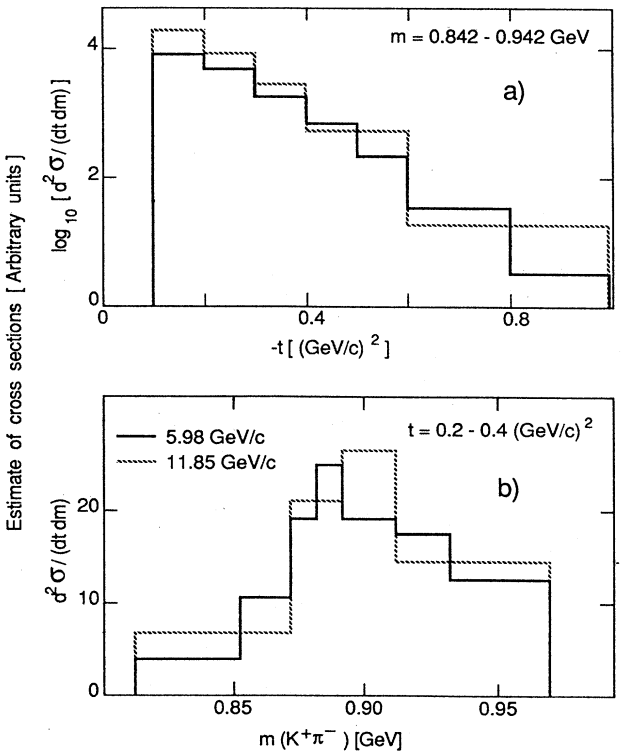

FIG. 5. Approximate results for the t dependence and the m dependence of the unpolarized cross section at 5.98 and 11.85 GeV/c. The units are arbitrary at both energies.

shown in Fig. 5. The relative normalization of different (t,m) bins was determined only approximately since it does not enter our analysis in terms of normalized observables in each bin.

IV. DATA ANALYSIS

The aim of the experiment is to determine the average values of normalized spin-density-matrix elements in small regions of four-momentum transfer squared $-t$ and dimeson invariant mass m. All events within a sufficiently small (t,m) bin are assumed to be produced with the same angular distribution $W(\theta,\varphi,\psi)$ (2.13).

In order to study both the t dependence and the m dependence of the $K^+\pi^-$ production amplitudes we have analyzed the same data in different sets of (t,m) bins. At 5.98 GeV/c (11.85 GeV/c) the t dependence is given in 7 (5) bins ranging from 0.1 to 1.0 $(\text{GeV}/c)^2$ and averaged over $(K^+\pi^-)$ mass from 0.842 to 0.942 GeV. The m dependence is given in 8 (4) bins ranging from 0.812 to 0.972 GeV and averaged over $-t$ from 0.2 to 0.4 $(\text{GeV}/c)^2$. An additional set was used at 5.98 GeV/c covering the entire region in 21 bins (7 t bins$\times$3 m bins). All of these results are presented in Tables IX to XIII of Ref. 14.

The method of maximum-likelihood function was used to determine the parameters $a_2,\ldots,a_{15}$ in the expression (2.15) from the accepted events in the bin (t,m). The construction of the maximum-likelihood function L, taking into account the acceptance of the apparatus and the relative normalization of successive runs with opposite signs of target polarization, is described in Ref. 7 for $\pi^+ n_\uparrow \to \pi^+\pi^- p$ but it also applies to the data analysis of $K^+ n_\uparrow \to K^+\pi^- p$. Since the data acquisition was simultaneous for both channels, the tests of stability for detection and reconstruction efficiencies, absolute momentum calibration of beam and forward spectrometer described in Ref. 7 are equally valid for the $K^+ n_\uparrow - K^+\pi^- p$ data. A limited study of sensitivity of our results to uncertainties in the acceptance integrals is described below.

Several consistency tests[7] were carried out using the S- and P-wave approximation for the angular distribution $W(\theta,\varphi,\psi)$ with unremarkable results. However, two special tests were performed at 5.98 GeV/c allowing for additional terms in the expansion for $W(\theta,\varphi,\phi)$.

(1) To search for parity-violating effects we added six terms proportional to imaginary parts of $\rho_{1s},\rho_{10},\rho_{1-1}$ and $\rho^\gamma_{1s},\rho^\gamma_{10},\rho^\gamma_{1-1}$.

(2) To search for D-wave effects we added six terms of higher order in θ proportional to linear combinations of interference terms between the dominating P- and D-wave amplitudes with dimeson helicities 0 or 1.

The results of these two tests deserve further comment.

The t dependence of the parity-forbidden imaginary parts in the K^{*0} mass region is shown in Fig. 6. The

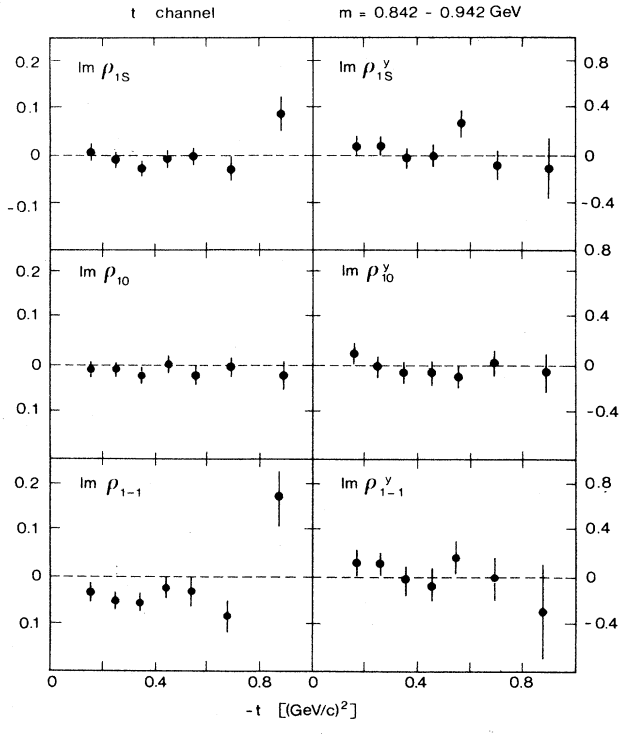

FIG. 6. Search for parity-violating effects. Parity-forbidden imaginary parts of SDM elements in the t channel at 5.98 GeV/c as a function of $-t$ in the K^{*0} mass region $m=0.842$–0.942 GeV.

nonzero values are generally small except in bins with small statistics. Of the first 14 parameters, the polarization-dependent ones shows greater change with respect to the results of the standard S- and P-wave analysis, in particular in bins with small statistics.[14] Figure 7 shows the change in polarized target asymmetry A which is the most affected parameter.

The t dependence of the P-D interference terms in the K^{*0} mass region is shown in Fig. 8. The polarization-dependent P-D terms are generally larger than the polarization-independent P-D terms. The polarization-dependent parameters $a_7, \ldots, a_{15}$ show again larger change than the polarization-independent parameters $a_2, \ldots, a_6$, in particular in bins with small statistics.[14] Figure 9 shows the change in polarized-target asymmetry A where, again, the change is largest.

Similar tests in our analysis of $\pi^+n_\uparrow \to \pi^+\pi^-p$ produced small values for parity-violating and P-D interference terms, and only negligible changes in the first 14 parameters.[7,14] However, in comparable t bins in the ρ^0 mass region, the statistics were larger by a factor of 3 to 6. We conclude that the apparent parity-violating and P-D interference effects both reflect low statistics and systematic errors in the apparatus or data analysis and do not indicate significant parity violation or large D wave in $K^+\pi^-$ production below 950 MeV. In the rest of this paper we will present and discuss only the results of the standard S- and P-wave analysis.

The relatively low statistics of the experiment imposes another limitation on our data analysis. The optimization of the maximum-likelihood function L should in principle take into account the constraints on the SDM elements imposed by positivity conditions[47–53] and nonlinear relations of La France-Winternitz type.[54] The hypothesis of S- and P-wave dominance introduces additional constraints. Imposing constraints during optimization involves methods of nonlinear programming,[58] and requires special optimization programs such as MINOS 5.0 developed at Stanford,[59] or others,[60] as well as special treatment of error matrix.[61] It is important to recognize

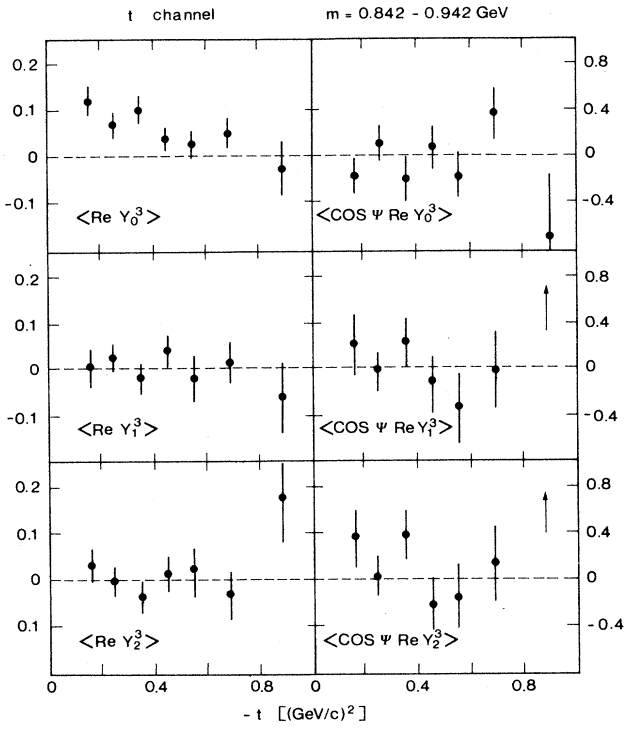

FIG. 8. Search for D-wave contributions. P- and D-wave interference terms in the t channel at 5.98 GeV/c as a function of $-t$ in the K^{*0} mass region $m = 0.842$–0.942 GeV.

that nonlinear relations between SDM elements are not valid for bin-averaged observables in bins of large size. Constrained analysis should be done in small (t,m) bins and this requires very high statistics in the experiment with acceptance calculations performed in the vicinity of each event. We anticipate that such high statistics will be achieved in the new generation of experiments at high-intensity accelerators.

The presented results were obtained by standard un-

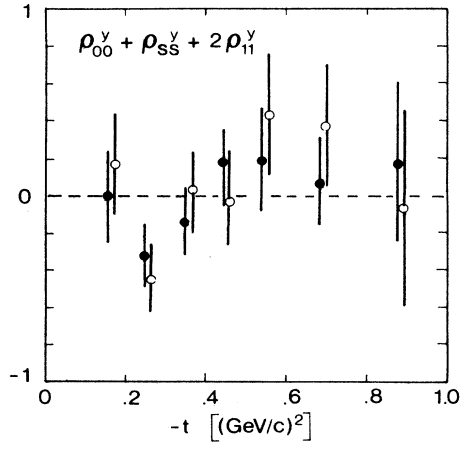

FIG. 7. Polarized-target asymmetry in the t channel at 5.98 GeV/c. Comparison of results in the absence (●) and in the presence (○) of the parity forbidden-imaginary parts of Fig. 6.

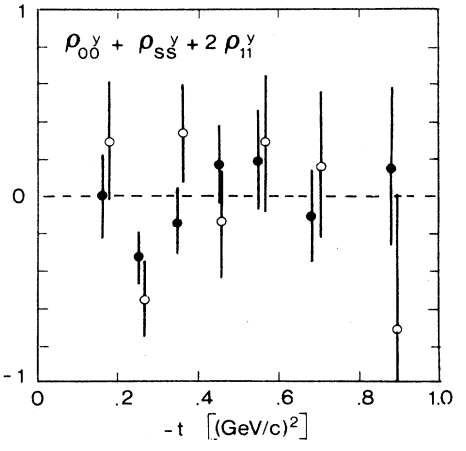

FIG. 9. Polarized target asymmetry in the t channel at 5.98 GeV/c. Comparison of results in the absence (●) and in the presence (○) of the P-D interference terms of Fig. 8.

constrained optimization. The CERN optimization program FUMILI was run at Saclay CDC 7600. The CERN program MINUIT yields essentially the same results.

The maximum-likelihood function $L = L(a,\epsilon)$ depends on the measured parameters a and on the acceptance integrals ϵ in any (t,m) bin. Whether the optimization is unconstrained or constrained, its solution point a^* is a function of the acceptance, $a^* = a^*(\epsilon)$. We performed a limited study of the response of the solution a^* to the estimated uncertainties in the acceptance integrals ϵ. We view the results of our sensitivity analysis as unremarkable and without evidence for catastrophic[62] or chaotic[63] behavior of a^*. However, we do suggest that this aspect of polarization measurements be more adequately addressed by the future designs for dedicated spin experiments with the aid of computer modeling.

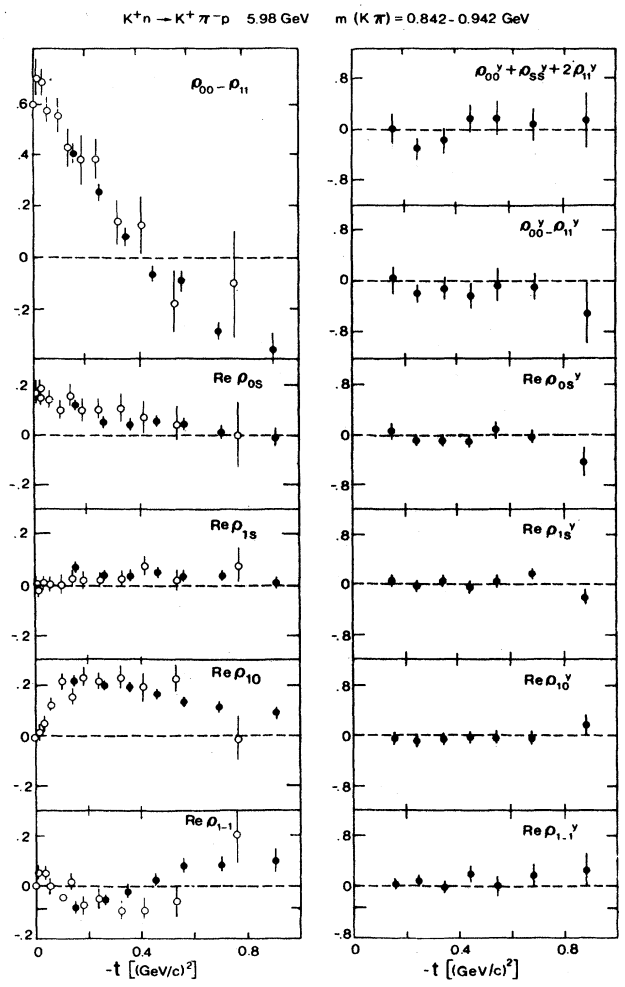

FIG. 10. Normalized spin-density-matrix (SDM) elements as a function of $-t$ in the $K^*(892)$ mass region at 5.98 GeV/c in the s-channel helicity frame. (a) Unpolarized SDM elements. The comparison is made with Argonne data (○) on unpolarized target at 6 GeV/c (Ref. 29). (b) Polarized SDM elements for transverse target nucleon polarization normal to the scattering plane. The scale for the polarized SDM elements is four times larger than the scale for unpolarized SDM elements.

V. EXPERIMENTAL RESULTS AND DISCUSSION

A. Spin-density matrix elements

Bin-averaged values of the 14 observed spin-density-matrix (SDM) elements were measured in small bins of (t,m) in both s- and t-channel dimeson helicity frames. The numerical results are all given in Ref. 14. Here we present figures only for selected results in the s channel.

Figure 10 shows the t dependence of SDM elements $a_2,\ldots,a_{12}$ in the K^{*0} mass region at incident momentum 5.98 GeV/c. We find a good general agreement with Argonne Zero Gradient Synchrotron (ZGS) data[29] for $K^+n \to K^+\pi^-p$ for unpolarized target at the same energy with a possible exception for ρ_{1-1} for $-t$ from 0.3 to 0.6 $(\mathrm{GeV}/c)^2$. The mass dependence of the same SDM elements averaged over the interval $-t = 0.2$–0.4 $(\mathrm{GeV}/c)^2$ is shown in Fig. 11. Figure 12 shows the t and m dependence of the SDM elements associated with $P_T \sin\psi$. Because of the limitations on acceptance in ψ,

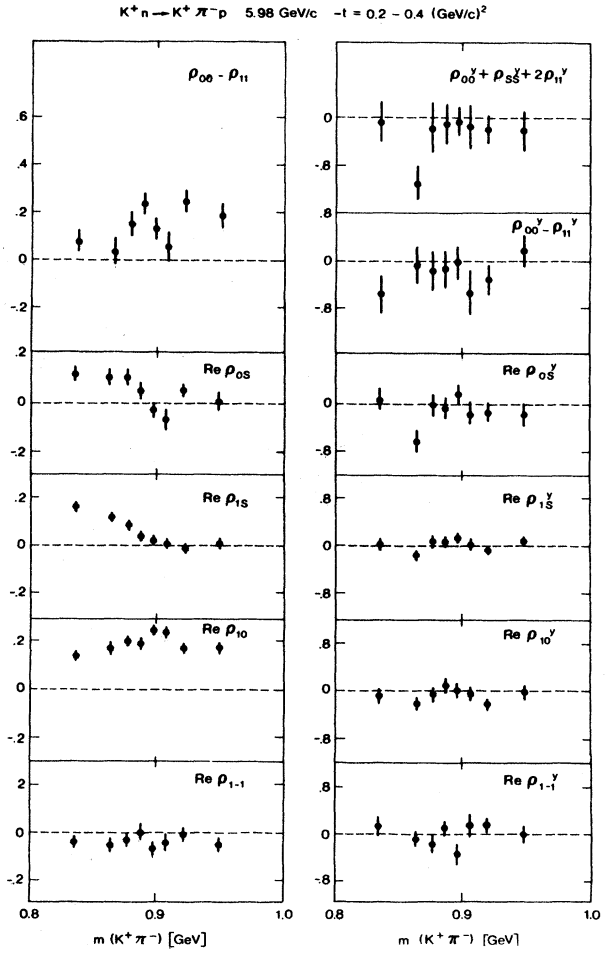

FIG. 11. Normalized spin-density-matrix (SDM) elements as a function of dimension mass m for $-t = 0.2$–0.4 $(\mathrm{GeV}/c)^2$ at 5.98 GeV/c in the s-channel helicity frame. (a) and (b) as in Fig. 10. The scale for the polarized SDM elements in four times larger than the scale for unpolarized SDM elements.

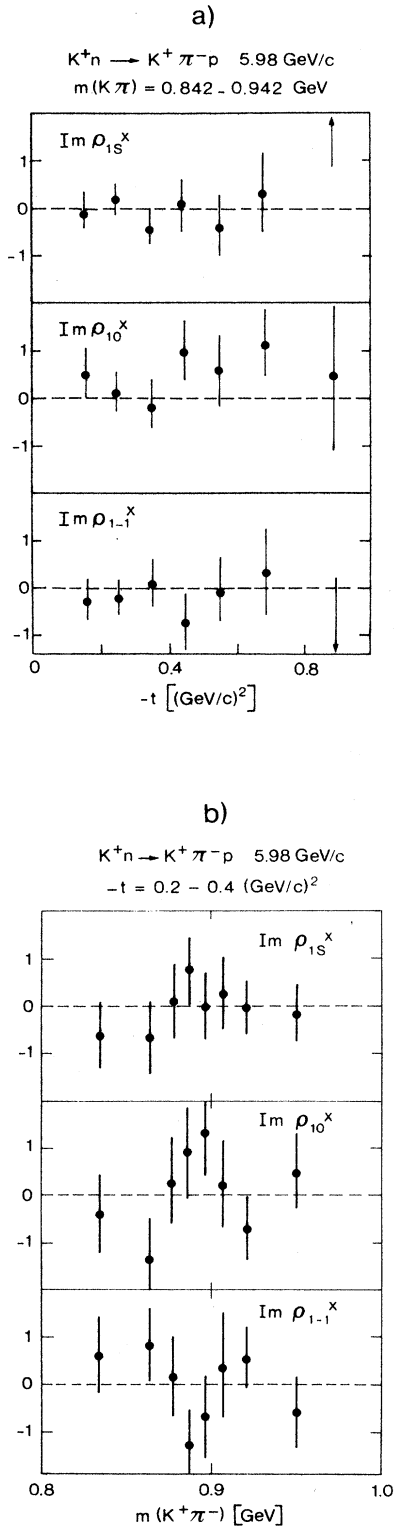

FIG. 12. Polarized spin-density-matrix elements ρ^x for transverse target nucleon polarization in the scattering plane measured at 5.98 GeV/c in the s-channel helicity frame. (a) The t dependence in the $K^*(892)$ mass region. (b) The mass dependence for $-t=0.2$–0.4 (GeV/c)^2.

these parameters are not well determined. The results at 11.85 GeV/c are similar within the larger errors due to lower statistics.

The t dependence of unpolarized SDM elements (2.21a) at K^{*0} mass can also be compared with the t dependence of similar π^-K^+ SDM elements in hypercharge-exchange reactions. The OMEGA spectrometer at the CERN PS was used to measure the π^-K^+ SDM elements in $\pi^-p \to \pi^-K+(\Lambda^0/\Sigma^0)$ at 10 GeV/c (Ref. 64) in the K^{*0} mass region. We note that the π^-K^+ SDM elements in this reaction have typically opposite sign. Also, $\mathrm{Re}\rho_{10}$ appears small in comparison to $\mathrm{Re}\rho_{10}$ in $K^+n_\uparrow \to K^+\pi^-p$ reaction. No information is available on the Λ^0 and Σ^0 polarization in this experiment.

In Secs. V B–V E we will make use of the fact that six of the measured SDM elements are simple linear combinations of the moduli squared of the eight nucleon transversity amplitudes defined in (2.18). Linear combinations of another six SDM elements measure relative phases between the unnatural-exchange amplitudes, and this information will be discussed in Secs. V F and V G.

B. Normalized partial-wave cross sections and recoil polarizations

The integrated cross section $d^2\sigma/(dm\,dt)$ was not measured in this experiment. Consequently, we will work with normalized nucleon transversity amplitudes corresponding to $\Sigma \equiv d^2\sigma/(dm\,dt)=1$, and define normalized partial-wave cross sections σ and partial-wave recoil polarizations τ for amplitudes $A=S,L,U,N$ as follows:

$$\sigma(A)=|A|^2+|\overline{A}|^2, \quad \tau(A)=|A|^2-|\overline{A}|^2 . \tag{5.1}$$

Some authors will prefer to call a partial-wave recoil polarization the ratio $P(A)=\tau(A)/\sigma(A)$. In our notation

$$\Sigma=\sigma(S)+\sigma(L)+\sigma(U)+\sigma(N)=1 \tag{5.2}$$

and

$$\begin{aligned}
&\rho_{ss}=\rho_{00}+2\rho_{11}=\sigma(S)+\sigma(L)+\sigma(U)+\sigma(N) ,\\
&\rho_{00}-\rho_{11}=\sigma(L)-\tfrac{1}{2}[\sigma(U)+\sigma(N)] ,\\
&\rho_{1-1}=-\tfrac{1}{2}[\sigma(U)-\sigma(N)] ,\\
&\rho^y_{ss}+\rho^y_{00}+2\rho^y_{11}=\tau(S)+\tau(L)+\tau(U)-\tau(N) ,\\
&\rho^y_{00}-\rho^y_{11}=\tau(L)-\tfrac{1}{2}[\tau(U)-\tau(N)] ,\\
&\rho^y_{1-1}=-\tfrac{1}{2}[\tau(U)+\tau(N)] .
\end{aligned} \tag{5.3}$$

Using the relations (2.14) we calculate from Eqs. (5.3) three mixed normalized partial-wave cross sections

$$\begin{aligned}
&\sigma(L)+\tfrac{1}{3}\sigma(S)=\tfrac{1}{3}[1+2(\rho_{00}-\rho_{11})] ,\\
&\sigma(U)+\tfrac{1}{3}\sigma(S)=\tfrac{1}{3}[1-(\rho_{00}-\rho_{11})]-\rho_{1-1} ,\\
&\sigma(N)+\tfrac{1}{3}\sigma(S)=\tfrac{1}{3}[1-(\rho_{00}-\rho_{11})]+\rho_{1-1} .
\end{aligned} \tag{5.4}$$

Similarly, from (5.3) we get three mixed partial-wave polarizations

$$\tau(L)+\tfrac{1}{3}\tau(S)=\tfrac{1}{3}[A+2(\rho^{y}_{00}-\rho^{y}_{11})]\,,$$
$$\tau(U)+\tfrac{1}{3}\tau(S)=\tfrac{1}{3}[A-(\rho^{y}_{00}-\rho^{y}_{11})]-\rho^{y}_{1-1}\,, \qquad (5.5)$$
$$-\tau(N)+\tfrac{1}{3}\tau(S)=\tfrac{1}{3}[A-(\rho^{y}_{00}-\rho^{y}_{11})]+\rho^{y}_{1-1}\,.$$

Figure 13 shows the results as a function of $-t$ in the K^{*0} mass region. We observe the expected dominance of $[\sigma(L)+\frac{1}{3}\sigma(S)]$ at small t and its decrease with t. For $|t|\gtrsim 0.6$ the natural-exchange contribution dominates. The mass dependence of observables (5.4) and (5.5) is shown in Fig. 14 for $0.2\le|t|\le 0.4$, and in Fig. 15 for $0.4\le|t|\le 0.5$. The polarization $[-\tau(N)+\frac{1}{3}\tau(S)]$ depends on both $-t$ and $p_{\rm lab}$. An analysis shows that the approximate equality of s- and t-channel values for $\sigma(L)$ and $\sigma(U)$ at $|t|<0.6$ is a kinematic effect.

To study in more detail the relative contribution of the natural exchange amplitudes we examine the ratio

$$R=\frac{\sigma(N)+\frac{1}{3}\sigma(S)}{\sigma(U)+\sigma(L)+\frac{2}{3}\sigma(S)}\,. \qquad (5.6)$$

This ratio does not depend on the choice of the s- or t-channel helicity frame of reference. The results of both energies are shown in Fig. 16. The natural exchange contribution increases linearly with t in the K^{*0} mass region. The mass dependence of R for $|t|=0.2$–0.4 $(\mathrm{GeV}/c)^2$ appears to change with energy.

C. The structure of nucleon transversity amplitudes

Equations (5.4) and (5.5) can be used to calculate the following combinations of moduli squared of nucleon transversity amplitudes:

$$|L|^2+\tfrac{1}{3}|S|^2,\quad |U|^2+\tfrac{1}{3}|S|^2,\quad |N|^2+\tfrac{1}{3}|\bar{S}|^2$$
$$|\bar{L}|^2+\tfrac{1}{3}|\bar{S}|^2,\quad |\bar{U}|^2+\tfrac{1}{3}|\bar{S}|^2,\quad |\bar{N}|^2+\tfrac{1}{3}|S|^2\,. \qquad (5.7)$$

Our results for (5.7) in both s and t-channel dimeson helicity frames are given in Ref. 14. Recall that the amplitudes $S,\bar{S},N,\bar{N}$ are invariant under s- to t-channel crossing transformation.

The results obtained from (5.7) can be taken as upper bounds on moduli squared of P-wave nucleon transversity amplitudes. The lower bounds are obtained by subtracting from the terms in (5.7) an upper bound on $\frac{1}{3}|S|^2$ or $\frac{1}{3}|\bar{S}|^2$. In each (t,m) bin we calculate

$$(\tfrac{1}{3}|S|^2)_{\rm upper}=\min_{\substack{A=L,U\\ s\text{ and }t}}\{|A|^2+\tfrac{1}{3}|S|^2,|\bar{N}|^2+\tfrac{1}{3}|S|^2\}\,,$$
$$(\tfrac{1}{3}|\bar{S}|^2)_{\rm upper}=\min_{\substack{A=L,U\\ s\text{ and }t}}\{|\bar{A}|^2+\tfrac{1}{3}|\bar{S}|^2,|N|^2+\tfrac{1}{3}|\bar{S}|^2\}\,. \qquad (5.8)$$

These upper and lower bounds allow an immediate discussion of the structure of the amplitudes in advance of detailed amplitude analysis. Since the bounds are given by linear combinations of the observables they also serve as a useful check on amplitude analysis[14] which is using equations for moduli that are nonlinear in the observables, and that may not be satisfied by the bin-averaged

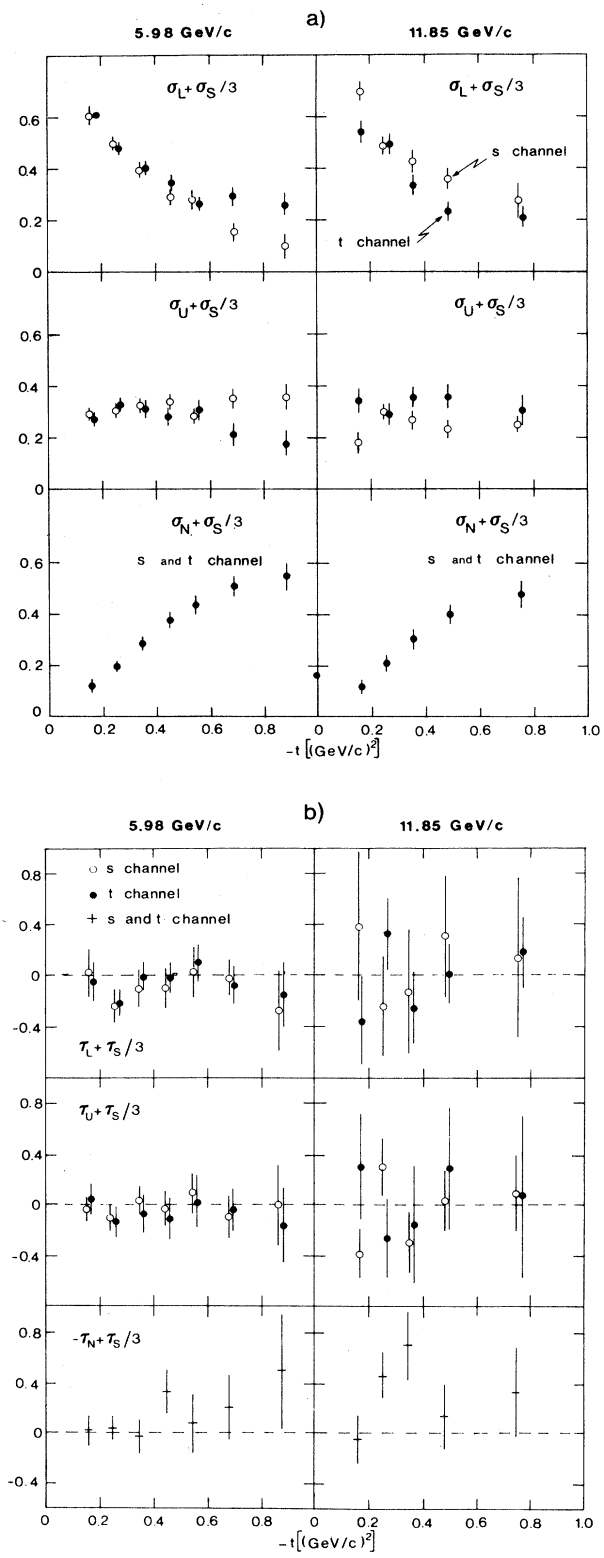

FIG. 13. The t dependence of linear combinations of (a) normalized partial-wave cross sections (b) partial-wave recoil polarizations in the K^{*0} mass region $m=0.842$–0.942 GeV at 5.98 and 11.85 GeV/c. Note that $\sigma(S)$, $\sigma(N)$, $\tau(S)$, and $\tau(N)$ are invariant under transformation from the t- to the s-channel dimeson helicity frame of reference.

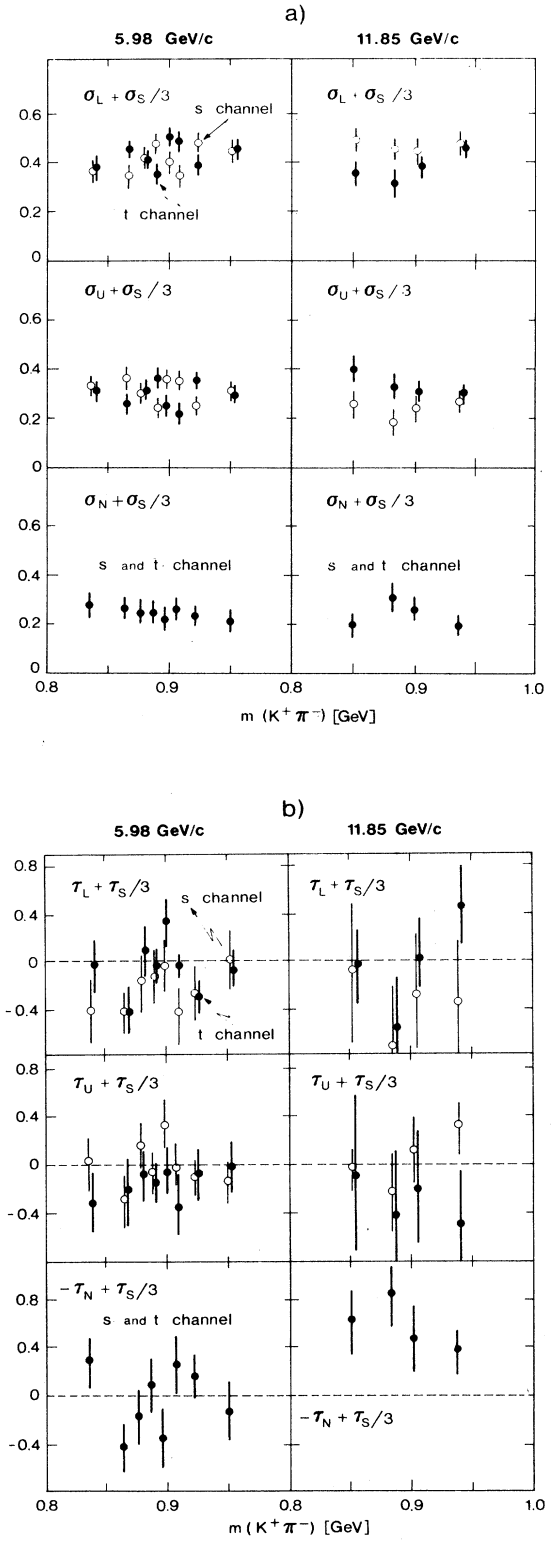

FIG. 14. The mass dependence of linear combinations of (a) normalized partial-wave cross sections and (b) partial-wave recoil polarizations for $-t=0.2$–0.4 $(\mathrm{GeV}/c)^2$ at 5.98 and 11.85 GeV/c.

values of the observables. The comparison of the two methods show consistency of their results. In particular, the moduli obtained in the exact amplitude analysis[14] are generally within the bounds (5.8).

Here we present our results for the bounds at 5.98 GeV/c. Figure 17 shows their t dependence at K^{*0} mass, while Figs. 18 and 19 show their mass dependence for $0.2 \le |t| \le 0.4$ $(\mathrm{GeV}/c)^2$ and $0.4 \le |t| \le 0.5$ $(\mathrm{GeV}/c)^2$, respectively. Only the mean values of the bounds are shown for clarity. The essential features of the amplitudes discussed below are valid within the statistical errors on the bounds.

Before we discuss our results for the bounds on moduli $|A|^2$ and $|\bar{A}|^2$ we note that in terms of the nucleon helicity-nonflip and -flip amplitudes A_n (2.17) these moduli are given by

$$\begin{aligned} 2|A|^2 &= |A_0|^2 + |A_1|^2 + 2\epsilon\,\mathrm{Im}(A_0 A_1^*)\,, \\ 2|\bar{A}|^2 &= |A_0|^2 + |A_1|^2 - 2\epsilon\,\mathrm{Im}(A_0 A_1^*)\,, \end{aligned} \tag{5.9}$$

where $\epsilon=+1$ for $A=S,L,U$ and $\epsilon=-1$ for $A=N$. When $|A|^2 \neq |\bar{A}|^2$ then both amplitudes A_0 and A_1 are nonzero and must have different phases. If $|A|^2 \simeq |\bar{A}|^2$ then either (a) one of the amplitudes A_0 and A_1 is small or vanishing, or (b) both amplitudes have the same phase. The sign of the relative phase between the nucleon helicity amplitudes is given by the sign of partial polarization

$$\tau(A) = |A|^2 - |\bar{A}|^2 = 2\epsilon |A_0||A_1| \sin(\phi_0 - \phi_1)\,. \tag{5.10}$$

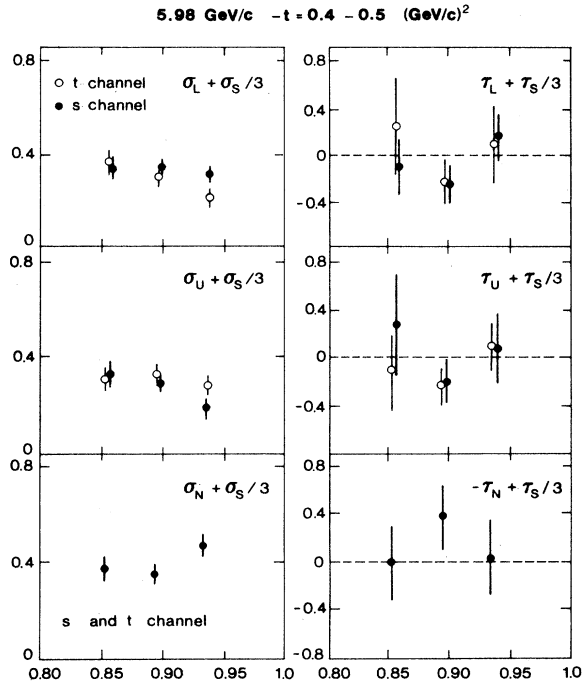

FIG. 15. The mass dependence of linear combinations of normalized partial-wave cross sections and partial-wave recoil polarizations for $-t=0.4$–0.5 $(\mathrm{GeV}/c)^2$ at 5.98 GeV/c.

We also recall that in the case of $K^+n \to K^+\pi^-p$ the unnatural-exchange helicity amplitudes A_n ($A = S, L, U$) are dominated by "A_1-Z" and "π-B" exchanges are $n=0$ and $n=1$, respectively. The natural-exchange amplitudes are dominated by "A_2-ρ" exchange for both $n=0,1$.

The bounds calculated from (5.7) and (5.8) are shown in Figs. 17, 18, and 19 and reveal several unexpected features of the spin dependence of the $K^+\pi^-$ state production.

The t dependence of moduli averaged over the broad mass range $m = 0.842$–0.942 GeV around the K^{*0} mass (Fig. 17) shows a decrease of $|L|^2$ and $|\bar{L}|^2$ with $-t$ as expected from the pion-exchange dominance of $\lambda=0$ amplitudes at small t. The $\lambda=\pm1$ unnatural exchange amplitudes $|U|^2$ and $|\bar{U}|^2$ are nearly constant, equal and relatively small throughout this region of t. The $K^+\pi^-$ state is produced predominantly with recoil transversity "up" via $|\bar{L}|^2$ (dimeson helicity $\lambda=0$) for $-t<0.4$ (GeV/c)^2 and via $|\bar{N}|^2$ (dimeson helicity $\lambda=\pm1$) for $-t>0.4$. We

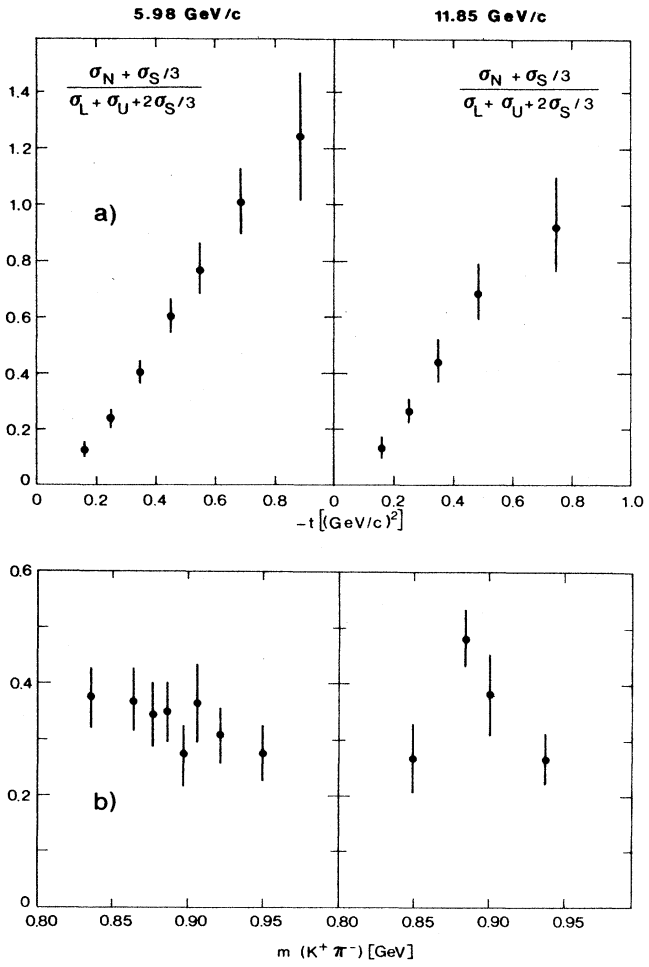

FIG. 16. The ratio of frame-invariant components of the cross section as a function of (a) $-t$ for $m = 0.842$–0.942 GeV and (b) dimeson mass m for $-t = 0.2$–0.4 (GeV/c).

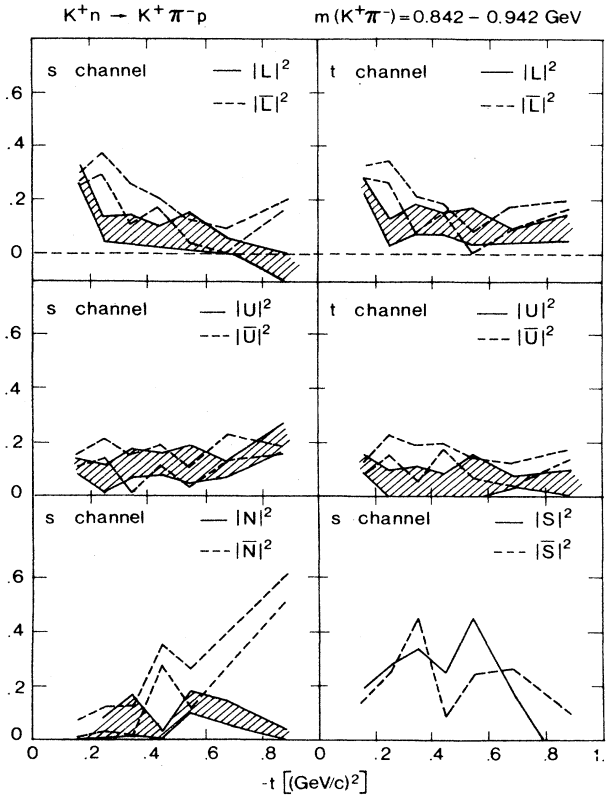

FIG. 17. The t dependence of the lower and upper bounds on the moduli squared of the normalized P-wave recoil transversity amplitudes for $m = 0.842$–0.942 GeV at 5.98 GeV/c. Also shown are the upper bounds on the moduli squared of the normalized S-wave amplitudes.

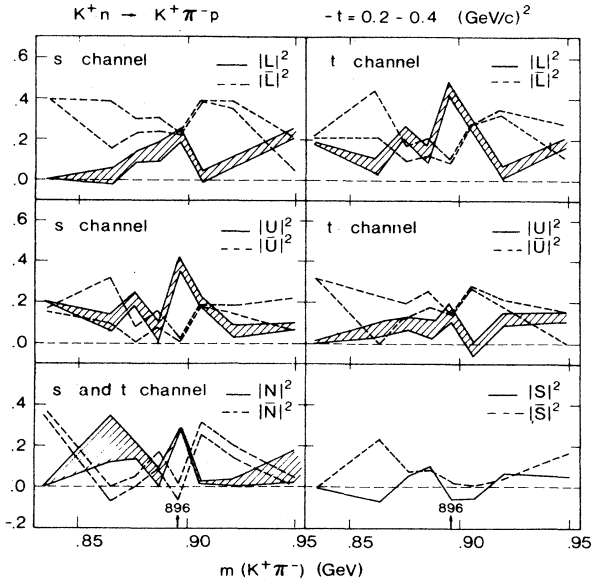

FIG. 18. The m dependence of the lower and upper bounds on the moduli squared of the normalized P-wave recoil transversity amplitudes for $-t = 0.2$–0.4 (GeV/c)^2 at 5.98 GeV/c, and the upper bounds on the moduli squared of the S-wave amplitudes.

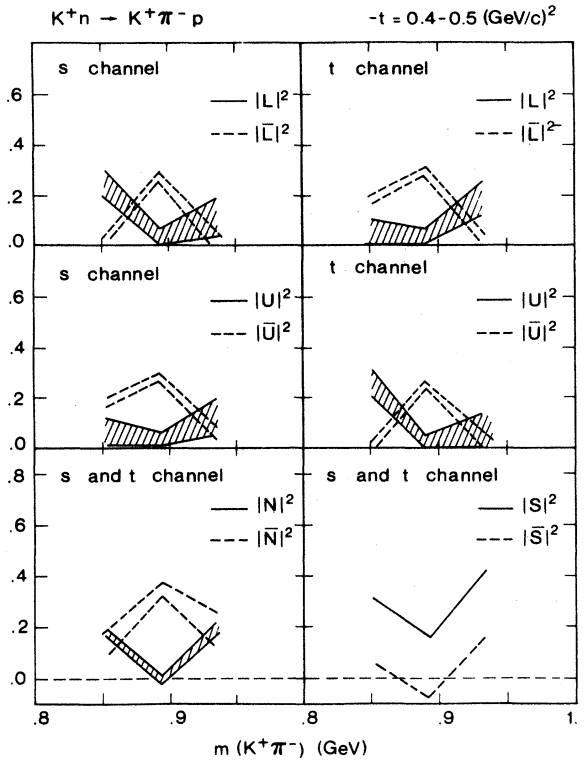

FIG. 19. Same as Fig. 18 for $-t=0.4$–0.5 (GeV/c)^2.

note that at $-t\simeq 0.4$ (GeV/c)^2 $|\bar{N}|^2$ is large but $|N|^2\simeq 0$. This indicates that, at this value of t, $|N_0|\simeq|N_1|$ with a relative phase of 90°. The relative phase $\psi_N=\psi_{N_0}-\psi_{N_1}$ is undergoing a 180° change between $-t=0.35$ and $-t=0.55$, going from $\psi_N\approx 0°$ for $-t\lesssim 0.3$ to $\psi_N\approx 180°$ at $-t\approx 0.55$, and to $\psi_N\approx 90°$ at $-t\approx 0.9$. In contrast, $\psi_U=\psi_{U_0}-\phi_{U_1}$ is small and nearly constant.

Figure 18 shows the mass dependence of moduli averaged over an interval of $-t=0.2$–0.4 (GeV/c)^2. This is the t region of largest statistics. In this study, the experimental resolution in m is of the same order as the bin width of mass m used in the Fig. 17.

The P-wave production of $K^+\pi^-$ state reveals a very intriguing mass dependence. In the s channel, $|L|^2\lesssim|\bar{L}|^2$ over the mass interval $m\approx 820$–940 MeV. The longitudinal $\lambda=0$ $K^+\pi^-$ state is thus produced predominantly with recoil transversity "up." At the K^{*0} mass $m=0.896$ GeV we observe $|\bar{L}|^2\approx|L|^2$, $|\bar{U}|^2\approx 0$, $|\bar{N}|^2\approx 0$ while $|U|^2$ and $|N|^2$ attain peak values with $|U|^2$ being the largest amplitude. Hence, in this range of t, the production of K^{*0} resonance with helicity $\lambda=0$ is independent of recoil transversity (transversities "up" and "down" are equally probable). However, the production of K^{*0} in helicity states $\lambda=\pm 1$ proceeds entirely with nucleon transversity "down" as the production with nuclear transversity "up" appears "forbidden." Near K^{*0} mass, the moduli of all normalized P-wave amplitudes with transversity "down" show a peak while those with the transversed "up" show a dip in both s- and t-channel helicity frames.

Figure 19 shows the mass dependence in the adjacent region of momentum transfer with $-t=0.4-0.5$ (GeV/c)^2. Here the production of K^{*0} proceeds almost entirely with the recoil transversity "up" for all K^{*0} helicity states, and it is the production with transversity "down" which is inhibited. Moreover, the K^{*0} production is almost independent of its helicity λ as $|\bar{L}|^2\approx|\bar{U}|^2\approx|\bar{N}|^2$.

In Fig. 18 we observe rapid changes in relative magnitudes of moduli $|U|^2$, $|\bar{U}|^2$ and $|N|^2,|\bar{N}|^2,|\bar{N}|^2$ within the mass interval $m=0.842$–0.942 GeV as we move away from the K^{*0} mass. Similar rapid changes are seen in Fig. 19 for all amplitudes. The closed-loop "diamond" structures characterizing these changes indicate either a 180° change in the relative phase $\psi_A=\psi_{A_0}-\psi_{A_1}$ of the corresponding helicity amplitudes, or that one of the helicity amplitudes vanishes at the nonresonant values of dimeson mass m where $|A|^2=|\bar{A}|^2$ (the crossover points). The present experiment cannot decide between these two alternatives.

We note in passing that the observed dip structures in the m dependence of moduli are due to the interference between flip helicity and -nonflip amplitudes at particular values of t. They should not be confused with resonant poles of second order.[65]

We now return to the t dependence of the natural contribution in the K^{*0} mass range (Fig. 17). The amplitudes $|N|^2$ and structure in the polarization $\tau(N)=|N|^2-|\bar{N}|^2$. The amplitudes $|N|^2$ and $|\bar{N}|^2$ in both reactions $K^+n\to K^+\pi^-p$ and $K^+n\to K^0p$ have "A_2-ρ" exchange structure. The polarization $P(K^+n\to K^0p)$ at 5.98 GeV/c also shows a clear double-zero structure at this value of t (Refs. 2 and 4).

D. The shape of K^{*0} peak in the physical region of t

The structures observed in the mass dependence of the P-wave recoil transversity amplitudes manifest themselves as differences in the shape of the K^{*0} peak in the unrenormalized partial-wave cross sections:

$$I(A)=\sigma(A)\frac{d^2\sigma}{dm\,dt},\quad A=L,U,N\ . \tag{5.11}$$

Since only $\sigma(A)+\frac{1}{3}\sigma(S)$ are directly measured [Eq. (5.4)], we define

$$K(A)=[\sigma(A)+\tfrac{1}{3}\sigma(S)]\frac{d^2\sigma}{dm\,dt},\quad A=L,U,N \tag{5.12}$$

and study also the shape effects in the differences involving P wave only:

$$\begin{aligned} &I(L)-I(U)=K(L)-K(U)\ ,\\ &I(L)-I(U)=K(L)-K(U)\ ,\\ &I(U)-I(N)=K(U)-K(N)\ . \end{aligned} \tag{5.13}$$

In terms of SDM elements, we get

$$I(L)-I(U)=[\tfrac{4}{3}(\rho_{00}-\rho_{11})+\rho_{1-1}]\frac{d^2\sigma}{dm\,dt}\ ,$$

$$I(L)-I(N)=[\tfrac{4}{3}(\rho_{00}-\rho_{11})-\rho_{1-1}]\frac{d^2\sigma}{dm\,dt}\ , \qquad (5.14)$$

$$I(U)-I(N)=-2\rho_{1-1}\frac{d^2\sigma}{dm\,dt}\ .$$

To evaluate (5.12) and (5.14) we used the approximate values of the cross section $d^2\sigma/dm\,dt$ shown in Fig. 5 at 5.98 GeV/c and for $-t=0.2-0.4$. The calculations were made in both s- and t-channel dimeson helicity frames and the results are shown in Figs. 20 and 21 for (5.12) and (5.14), respectively. The typical errors are shown in Fig. 21 for I_U-I_N.

In the s channel, $I_L+\frac{1}{3}I_S$ has a pronounced K^{*0} peak near 887 MeV while $I_U+\frac{1}{3}I_S$ is broader, less pronounced, and near 897 MeV. In the t channel, $I_L+\frac{1}{3}I_S$ still dominates but it has a broader peak near 897 MeV while $I_U+\frac{1}{3}I_N$ is narrower and the apparent position is shifted towards 887 MeV. The crossing invariant $I_N+\frac{1}{3}I_S$ has a peak near 887 MeV over a broad background. These effects are due to the P wave and not to the S wave. This is best verified by the S-wave independent differences (5.14) shown in Fig. 21. The statistical significance of these effects is illustrated in the figure for I_U-I_N which shows the error bars.

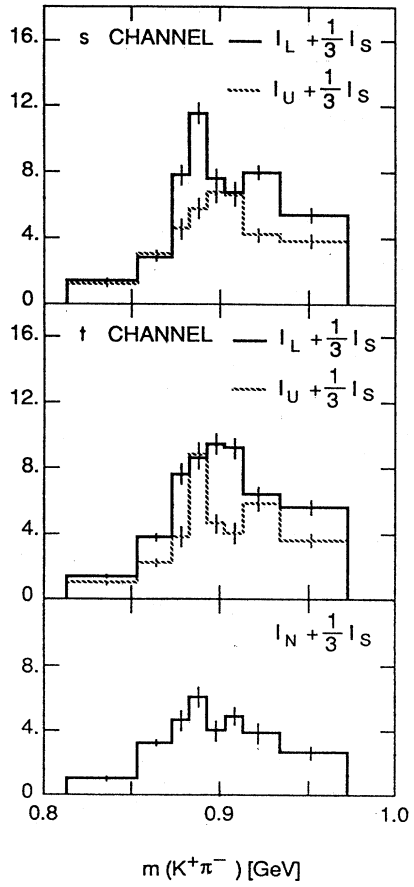

FIG. 20. The m dependence of three components of unnormalized cross section $d^2\sigma/dm\,dt$ for $-t=0.2-0.4$ (GeV/c)^2 at 5.98 GeV/c. The arbitrary units are the same as in Fig. 5.

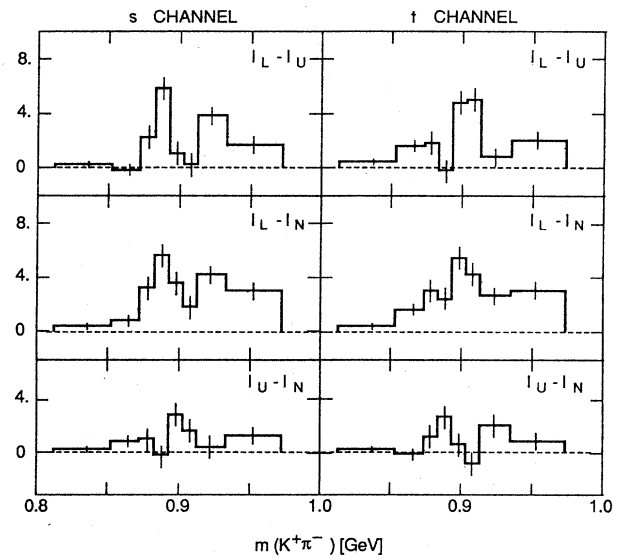

FIG. 21. The S-wave independent differences of unnormalized partial-wave cross sections for $-t=0.2-0.4$ (GeV/c)^2 at 5.98 GeV/c in the s- and t-channel dimeson helicity frames of reference. The arbitrary units are the same as in Fig. 5.

The shifts in the apparent position of the K^{*0} peak and the variations of its width are t dependent. Similar effects were also observed[7] for ρ^0 peak in $\pi^+ n_\uparrow \to \pi^+\pi^- p$ at 5.98 and 11.85 GeV/c.

To understand qualitatively the origin of these differences in the apparent position and shape of the K^{*0} peak in the partial-wave cross sections, let us consider any P-wave nucleon transversity amplitude $A(s,t,m^2)$ as a function of the complex dimeson mass squared z. In the real vicinity of the K^{*0} complex pole $Z_{K^*}=m^2_{K^*}-i\delta$ we can write

$$A(s,t,m^2)=\frac{R(s,t,Z_{K^*})}{m^2-Z_{K^*}}+Q(s,t,m^2)\ , \qquad (5.15)$$

where $R(s,t,Z_{K^*})$ is the pole residue and $Q(s,t,m^2)$ the background analytic near Z_{K^*}. The pole residue can be factorized

$$R=F(s,t,Z_{K^*})f(Z_{K^*})\ , \qquad (5.16)$$

where F and f are amplitudes for $K^+n\to K^{*0}p$ and $K^{*0}\to K^+\pi^-$, respectively. The residues R modulate the width of the resonance peak in each transversity amplitude A. The interference of the pole term with the background term can produce the small shifts in the apparent position of the K^{*0} peak discussed above. These effects vary with s and t. In contrast with the quasi-two-body amplitudes $F(s,t,Z_{K^*})$, the dynamical content of the background contributions is much less understood, e.g., in terms of Regge exchanges or coherent contributions from competing processes leading to $K^+\pi^-p$ final state.[66,67]

We conclude that the apparent position and the apparent width of K^{*0} resonance in partial-wave cross sections depend dynamically on the dimeson helicity, exchange naturality, helicity frame and vary with s and t.

E. Test of additive-quark-model predictions

The reactions $K^+n \to K^{*0}p$ and $pp \to \Delta^{++}n$ are both exotic in the s channel and exchange the same t-channel quantum numbers: ρ-A_2 natural-parity exchanges, and π-B and A_1-Z unnatural-parity exchanges. In general, the reaction $pp \to \Delta^{++}n$ is described by 16 helicity amplitudes. The additive quark model (AQM) (Refs. 68 and 69) reduces this number to 6 and relates these remaining amplitudes to those in $K^+n \to K^{*0}p$ at the same value of t. These relations between amplitudes lead to relations between SDM elements in the two reactions. When the reactions $K^+n_\uparrow \to K^{*0}p$ and $p_\uparrow p \to \Delta^{++}n$ are measured on a polarized target and with a polarized proton beam, respectively, the AQM predictions for SDM elements read

$$\sigma_L \equiv \rho_{00} = 2(\rho_{11} - \tfrac{1}{3}\rho_{33}) , \tag{5.17}$$

$$\sigma_U \equiv \rho_{11} - \rho_{1-1} = \tfrac{4}{3}(\rho_{33} - \sqrt{3}\rho_{3-1}) , \tag{5.18}$$

$$\sigma_N \equiv \rho_{11} + \rho_{1-1} = \tfrac{4}{3}(\rho_{33} + \sqrt{3}\rho_{3-1}) , \tag{5.19}$$

$$\mathrm{Re}\rho_{10} = \left[\frac{4}{\sqrt{6}}\right]\rho_{3-1} , \tag{5.20}$$

$$\mathrm{Im}\rho_{10} = -\frac{1}{\sqrt{2}}\rho^y_{11} , \tag{5.21}$$

where the left-hand side (LHS) and RHS refer to K^{*0} and Δ^{++} production, respectively.[70]

Notice that the polarization-dependent SDM elements measured in $K^+n_\uparrow \to K^{*0}p$ do not enter explicitly into the comparison with SDM elements measured in $p_\uparrow p \to \Delta^{++}n$. The reason is that the former SDM elements are interference terms $A_0 A_1^*$ between $n=0,1$, amplitudes of the same kind. Such interferences are not measurable in $p_\uparrow p \to \Delta^{++}n$ and require polarized target observables in $pp_\uparrow \to \Delta^{++}n$ with Δ^{++} produced forward.[71]

Because of P-parity conservation $\mathrm{Im}\rho_{10}$ is not accessible to observation in any type of polarization measurements in $KN \to K\pi N$. Thus its connection (5.21) to the measured $\rho^y_{11}(\Delta)$ cannot be directly tested. The observable $\mathrm{Re}\rho_{10}$ is measured directly and (5.20) is directly testable. To test the predictions (5.17)–(5.19) we used estimates of the upper and lower bounds on the normalized partial wave cross sections $\sigma(A)$, $A = L, U, N$ in a way similar to (5.8). The upper bounds are obtained by linear combinations of measured quantities (5.4):

$$\sigma(A)_{\mathrm{upper}} \equiv \sigma(A) + \tfrac{1}{3}\sigma(S) . \tag{5.22}$$

The lower bounds on $\sigma(A)_{\mathrm{upper}}$ are obtained by subtracting from $\sigma(A)_{\mathrm{upper}}$ an upper bound on $\frac{1}{3}\sigma(S)$:

$$\sigma(A)_{\mathrm{lower}} = \sigma(A)_{\mathrm{upper}} - \tfrac{1}{3}\sigma(S)_{\mathrm{upper}} , \tag{5.23}$$

where

$$\tfrac{1}{3}\sigma(S)_{\mathrm{upper}} = \min_{\substack{A=L,U,N \\ s \text{ and } t}} [\sigma(A) + \tfrac{1}{3}\sigma(S)] . \tag{5.24}$$

The AQM predictions are tested for SDM elements defined in the t-channel helicity frame. The data for $p_\uparrow p \to \Delta^{++}n$ at 6 GeV/c incident momentum[23] are compared in Fig. 22 to our data at 5.98 GeV/c for $m(K^+\pi^-) = 0.842$–0.942 GeV as a function of t. There is a remarkable agreement for (5.20) involving $\mathrm{Re}\rho_{10}$. The agreement for other AQM predictions is also reasonable. The observed deviations from AQM model may have a kinematic origin[69] or may reflect a diquark component in the baryon structure.[72–74] We note that spin rotation of hadron wave function on scattering gives rise to hadron spin flip even when the underlying quark-quark amplitudes conserve helicity.[75]

Model-independent amplitude analysis of $K^+n_\uparrow \to K^+\pi^-p$ enables a more detailed test of AQM predictions, including the prediction (5.21) using bounds based on the positivity of SDM (Ref. 15).

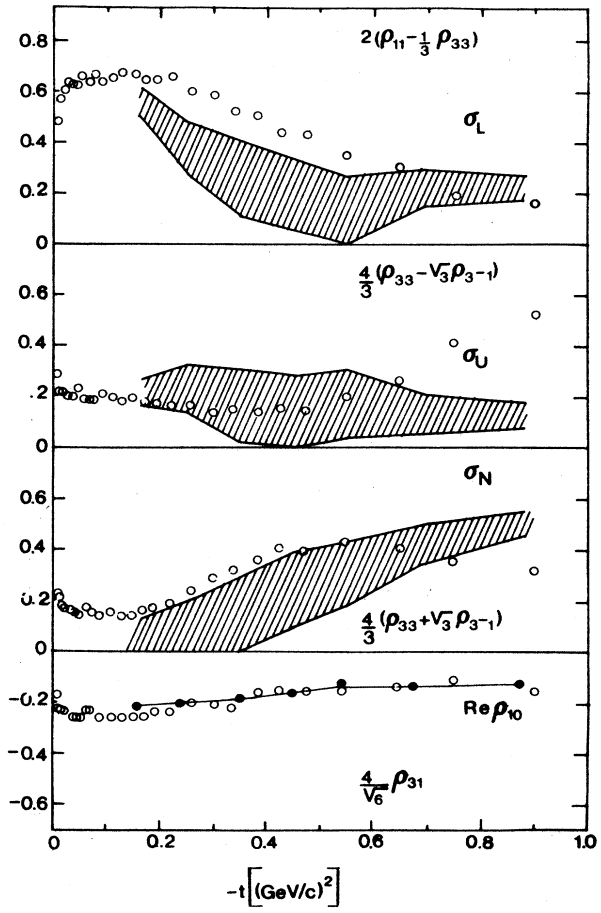

FIG. 22. Test of four additive quark-model predictions relating spin-density-matrix elements in reactions (a) $K^+n \to K^{*0}p$ and (b) $pp \to \Delta^{++}n$. The bounds and solid points are the terms from the reaction (a), the open circles are the terms from the reaction (b) in the t-channel helicity frames. The model predicts equality of the terms (a) and (b).

F. Test of assumptions in phase-shift analyses of $K\pi \to K\pi$ scattering

To perform a phase-shift analysis of $K\pi \to K\pi$ scattering using an extrapolation of $KN \to K\pi N$ unpolarized data into unphysical region of t, the enabling assumptions (1.1) or (1.2) are required. In our notation Eqs. (1.1) and (1.2) read

$$A_0 = 0 \ , \tag{1.1'}$$

$$A_0 = cA_1 \ , \tag{1.2'}$$

where $A = S, L, U$. In terms of the nucleon transversity amplitudes these relations are equivalent to

$$A = \overline{A} \ , \tag{1.1''}$$

$$A = \left[\frac{c+i}{c-i}\right]\overline{A} \ . \tag{1.2''}$$

The analysis of unpolarized data using the assumptions (1.2) differs from the analysis using (1.1) only by normalization factor $\sqrt{1+|c|^2}$ for the magnitudes of the amplitudes. The behavior of phase shifts is the same in both analyses.

The assumptions (1.1) and (1.2) lead to testable predictions for polarized SDM elements. The hypothesis (1.1) implies

$$\rho^{y}_{SS} + \rho^{y}_{00} + 2\rho^{y}_{11} = -2(\rho^{y}_{00} - \rho^{y}_{11}) = +2\rho^{y}_{1-1}$$
$$= 2\,\mathrm{Im}(N_0 N_1^*) \ , \tag{5.25}$$

$$\mathrm{Re}\rho^{y}_{10} = \mathrm{Re}\rho^{y}_{1s} = \mathrm{Re}\rho^{y}_{0s} = 0 \ . \tag{5.26}$$

The predictions of (1.2) read

$$0 < \frac{\rho_{10} - \rho^{y}_{10}}{\rho_{10} + \rho^{y}_{10}} = \frac{\rho_{1s} - \rho^{y}_{1s}}{\rho_{1s} + \rho^{y}_{1s}} = \frac{\rho_{0s} - \rho^{y}_{0s}}{\rho_{0s} + \rho^{y}_{0s}} = r \ , \tag{5.27}$$

where

$$r = \frac{|c-i|^2}{|c+i|^2} \ . \tag{5.28}$$

Note that (5.26) leads to $r = 1$.

Our data for polarized SDM elements in Figs. 10 and 11 clearly rule out the predictions (5.25) and (5.26). To test (5.27), all sums and differences are shown in Figs. 23, 24, and 25 in the s channel. While the first ratio of (5.27) is positive, the second and third ratios are negative in the vicinity of K^{*0}, seriously contradicting (5.27).

We conclude that the information from polarized SDM elements is not contained in the existing phase-shift analyses of $K\pi \to K\pi$ scattering. We suggest that incorporating this information into phase-shift analyses is very important for hadron spectroscopy. We suspect that some old conclusions may be revised.

G. The structure of S wave in $K^+\pi^-$ production

The production of $K^+\pi^-$ in the pure $J=0$ spin state is described by the amplitudes S and $\bar{S}$. The experimental knowledge of these amplitudes is essential in the search for scalar resonances below 1000 MeV. We gain some in-

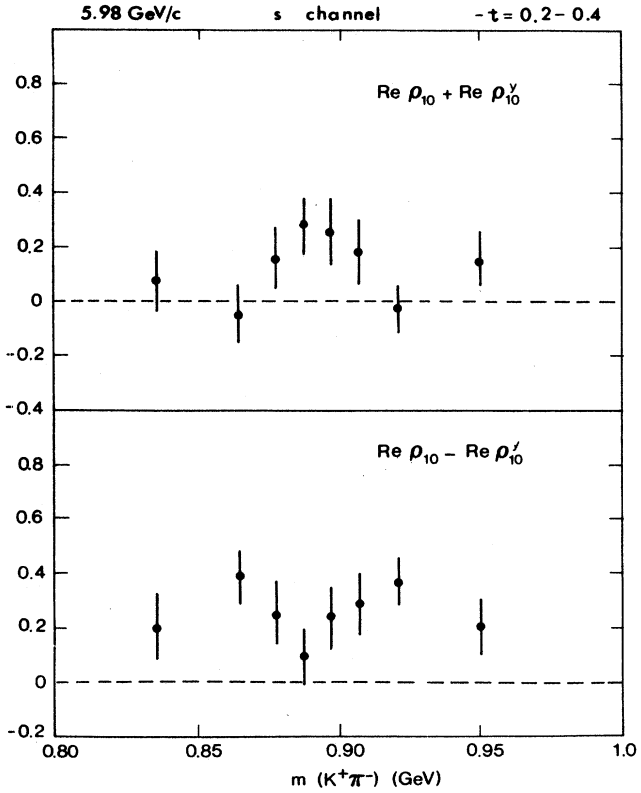

FIG. 23. Interference terms of definite transversity between P-wave amplitudes L and U in the s channel as a function of dimeson mass for $-t = 0.2$–0.4.

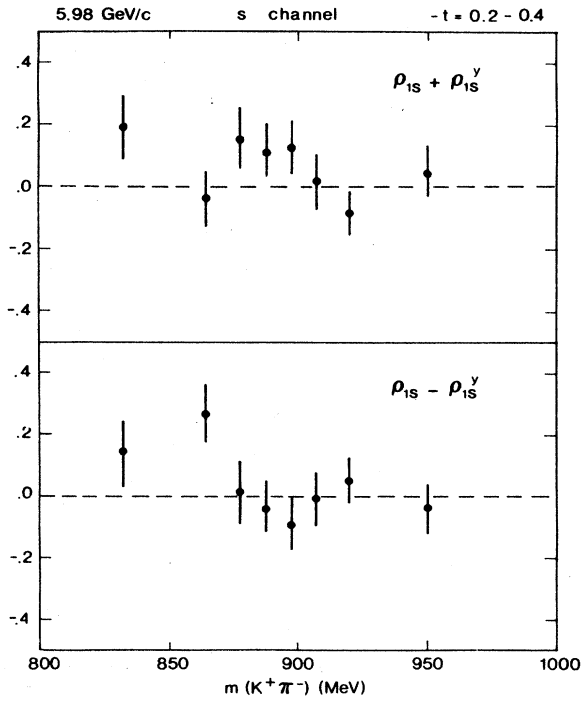

FIG. 24. The S-P-wave interference terms of definite transversity between amplitudes S and U in the s channel as a function of dimeson mass for $-t = 0.2$–0.4.

sight into the S-wave amplitudes by examining the S-P-wave interference terms:

$$\begin{aligned} &\mathrm{Re}\rho_{0s} + \mathrm{Re}\rho^{y}_{0s} = 2|S||L|\cos(\gamma_{SL}) , \\ &\mathrm{Re}\rho_{0s} - \mathrm{Re}\rho^{y}_{0s} = 2|\bar{S}||\bar{L}|\cos(\bar{\gamma}_{SL}) , \end{aligned} \tag{5.29}$$

$$\begin{aligned} &\mathrm{Re}\rho_{1s} + \mathrm{Re}\rho^{y}_{1s} = \sqrt{2}|S||U|\cos(\gamma_{SU}) , \\ &\mathrm{Re}\rho_{1s} - \mathrm{Re}\rho^{y}_{1s} = \sqrt{2}|\bar{S}||\bar{U}|\cos(\bar{\gamma}_{SU}) . \end{aligned} \tag{5.30}$$

The polarization measurements thus provide a separation of contributions from amplitudes with opposite transversities. The results are shown in Figs. 24, 25, and 26.

In the K^{*0} mass interval the interferences (5.29) and (5.30) show similar behavior for amplitudes of the same transversity in both s and t channels. Although $\cos\gamma$ and $\cos\bar{\gamma}$ have opposite signs, the interferences for amplitudes of opposite transversities also have similar structure: peak values near 897 MeV and change of sign at ≈ 880 and ≈ 910 MeV. These structures are consistent with a 180° phase change in γ and $\bar{\gamma}$ associated with a resonant P wave and a nonresonant smooth S wave near K^{*0}.

Our data for the dimeson mass $\lesssim 880$ MeV suggest a repetition of this pattern with opposite signs and with the peak values near 860 MeV. Such behavior is consistent with a hypothesis assuming a nonresonant P wave and a weak $I = \frac{1}{2}$ S-wave resonance $0^{++}(860)$ with a width of 20–40 MeV. Such state was previously suggested on theoretical grounds[76] and was possibly seen already in previous measurements of $K^-p \to K^-\pi^+n$ (Ref. 77), $K^+n \to K^+\pi^-p$ (Ref. 78), and $K^-p \to K^0\pi^-p$ (Ref. 79) at smaller values of t.

We cannot claim conclusive evidence for the $I = \frac{1}{2}$ $0^{++}(860)$ state in our experiment since the inference is based primarily on the first three data points in Figs. 25 and 26. By the same token, we cannot truly rule out a scalar state under $K^{*0}(890)$, since the disclaimer is based primarily on the next three data points in the same figures. However, our data should inspire new experiments with spin dedicated to search for a possible scalar state near or below the K^{*0} mass.

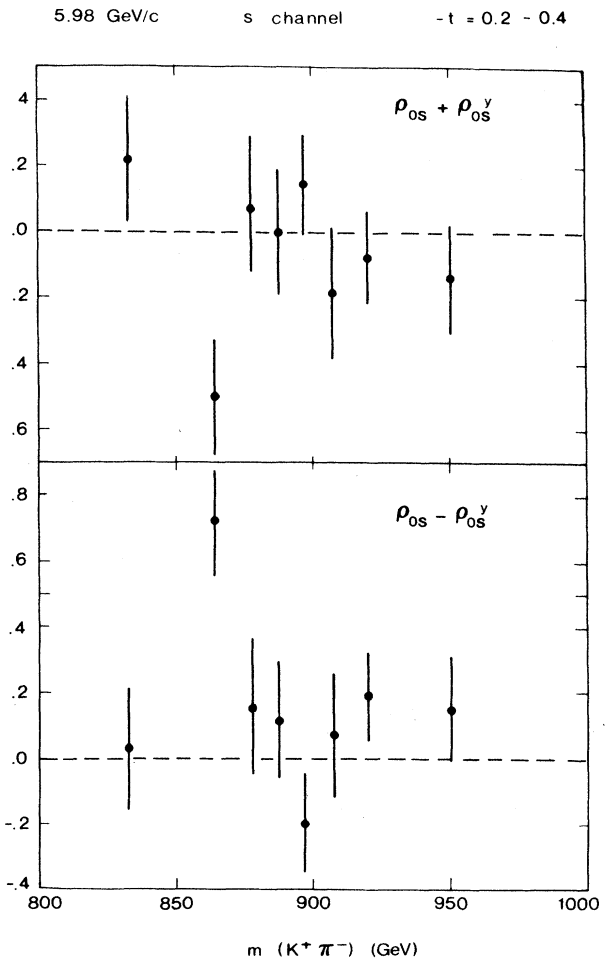

FIG. 25. The S-P-wave interference terms of definite transversity between amplitudes S and L in the s channel.

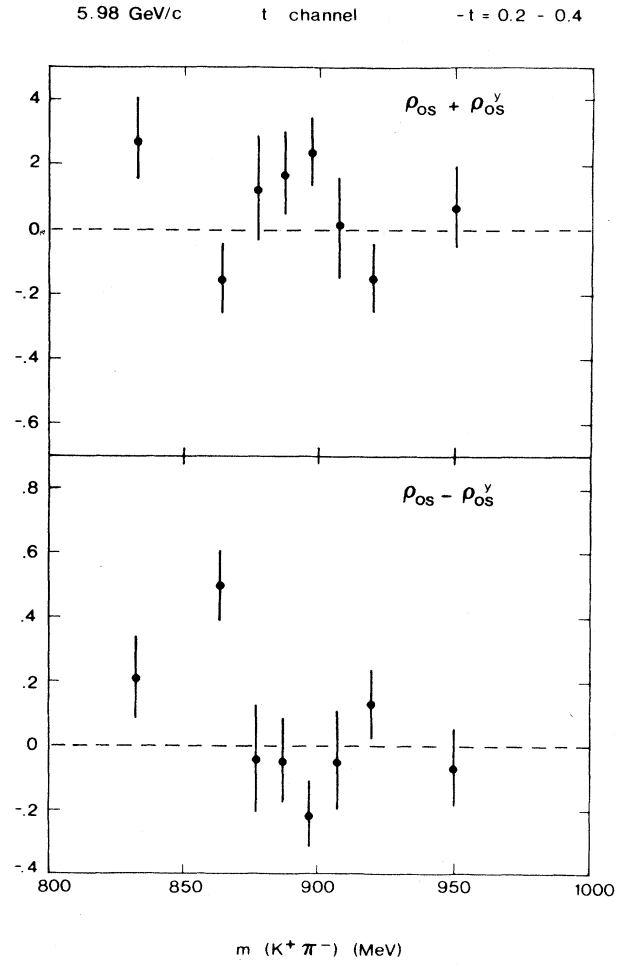

FIG. 26. The S-P-wave interference terms of definite transversity between amplitudes S and L in the t channel.

VI. CONCLUSIONS

In this first experiment on pion production in $K^+ n_\uparrow \to K^+ \pi^- p$ with transversely polarized quasifree neutron target we measured 14 spin-density-matrix elements in small (t,m) bins at 5.98 and 11.85 GeV, in both s- and t-channel helicity frames. From these data we determined three mixed normalized partial-wave cross sections (5.4) and recoil nucleon polarizations (5.5). These results were then used to construct moduli squared of P-wave nucleon transversity amplitudes with an admixture of one-third of S-wave moduli squared [Eq. (5.7)]. To study the structure of P-wave moduli, we have isolated them by constructing lower and upper bounds (5.8). The sums and differences (2.22b) isolate interferences between amplitudes of the same transversity and provide some information about cosines of certain relative phases. We have also performed a detailed amplitude analysis[14] which will be reported elsewhere.

We find only a weak energy dependence when comparing the results for the mixed normalized partial-wave cross sections (5.4) and recoil polarizations (5.5) at 5.98 and 11.85 GeV/c. A comparison of partial-wave cross sections with the corresponding results for the reaction $\pi^+ n_\uparrow \to \pi^+ \pi^- p$ shows a certain similarity in their t dependence at resonant masses. This is consistent with an SU(3) invariance of t-channel exchanges, in spite of additional contributions from the B, Z, and ρ exchanges permitted in $KN \to K\pi N$. A comparison of the t dependence of the mixed partial-wave recoil polarizations in the two reactions shows differences which can be attributed to the ρ-exchange contribution in $KN \to K\pi N$.

The mass dependence of the observables (5.12) and (5.14) reveals that the apparent position and the apparent width of K^{*0} resonance in the partial-wave cross section depend on dimeson helicity and t-channel naturality. Similar observations were found in the case of ρ^0 production in $\pi^+ n_\uparrow \to \pi^+ \pi^- p$ reaction.[7]

Although the nucleon spin-averaged partial-wave cross sections are relatively smooth, the moduli of individual recoil transversity amplitudes show strong and systematic structures in their mass dependence in the studied intervals of momentum transfer $-t = 0.2-0.4$ (GeV/c)^2 and $-t = 0.4-0.5$ (GeV/c)^2. The study of t evolution of mass dependence in $\pi^+ n_\uparrow \to \pi^+ \pi^- p$ also reveals unexpected structures in the production amplitudes.[7,8] These observations show that isolating the nucleon-spin states experimentally is as important as isolating the dimeson helicities and t-channel naturalities. We conclude that attempts to understand resonance production from nucleon-spin-averaged observables alone are very likely to miss some essential aspects of the dynamics.

Our experiment provides clear evidence for "A_1-Z" unnatural-exchange signal in $KN \to K\pi N$ reaction (Figs. 18 and 19). Partial-wave analyses of meson-meson scattering based on extrapolations to unphysical region of unpolarized pion production data require the enabling assumptions (1.1) or (1.2). Both assumptions lead to predictions for polarized SDM elements which are clearly contradicted by our data. The nucleon helicity nonflip amplitudes in pion production do not have the trivial behavior assumed by those analyses, at least not in the kinematic region of our experiment. We conclude that partial-wave analyses of $K\pi \to K\pi$ scattering do not contain the important information from the measurements of $KN \to K\pi N$ with spin and are thus open to revisions.

We used our data at 5.98 GeV/c and the high-statistics Argonne data on $p_\uparrow p \to \Delta^{++} n$ at 6 GeV/c to test the predictions of additive quark model which relates the amplitudes and thus the SDM elements in the two reactions. There is a remarkable overall agreement. The systematic deviations from AQM may have a dynamical origin.

Our data on the polarized SDM elements at 5.98 GeV/c suggest the possible existence of a new scalar resonance $I = \frac{1}{2}\ 0^{++}(860)$ with a width of 20–40 MeV. However suggestive, the evidence is not conclusive.

Finally, we comment briefly on the outlook for a new generation of meson production experiments with spin.

Experiments with polarized targets have opened a whole new approach to experimental hadron spectroscopy. Measurements of spin-dependent observables enable model-independent partial or complete amplitude analyses. The production of known dominant resonances can thus be studied on the level of production amplitudes, rather than cross sections, and in the physical region of m and t. The "nonresonating" amplitudes may reveal subdominant resonances that now may be hidden in the spin-averaged cross sections. Such a search is of particular relevance to QCD with its predictions of new hadron matter—gluonium states (gg,ggg), hybrid states ($q\bar{q}g$), and meson molecules ($\pi\pi$,$K\pi$). The importance of experimental hadron spectroscopy on the level of amplitudes was recently emphasized in several papers.[80–83]

The results of our experiment indicate an urgent need for a new generation of dedicated experiments with spin to explore in detail the spin dependence of pion production near and away from the resonant masses; to search for possible new scalar resonances such as $0^{++}(860)$ and to clarify the questions of D-wave contribution and parity conservation in pion production. The designs of these dedicated experiments must take into account the advances in constrained optimization and determine the response of the polarized SDM elements to the uncertainties in the calculated acceptance of the apparatus. To treat these aspects, the designers should find useful the new technologies of computer-aided design and computer modelling.

A new generation of experiments with spin dedicated to precise amplitude analyses and hadron spectroscopy will benefit from important recent advances in polarized targets, such as wide-angle acceptance,[84] fast orientability of target polarization into any direction,[85] and new radiation-resistant materials with lower unpolarized background.[86,87] Polarized jet targets offer the important advantage of no unpolarized background.[88–90] New high intensity accelerators have been proposed specifically for high-precision experiments with pion, kaon, and antiproton beams[91–97] in the multi-GeV region. These advanced hadron facilities will also provide high-quality polarized proton beams[95] and enable construction of secondary polarized beams of hyperons, antiprotons, and leptons.[98] Very attractive is the possibility of polarizing stored an-

tiproton beams,[99] which would allow complete amplitude analyses of pion production reactions in crossed channels: $\bar{N}N \to \pi^+\pi^-\pi^0$, $K^+K^-\pi^0$, etc. As the measurements of the recoil nucleon polarization are difficult, the direct channel experiments will utilize the self-analyzing properties of hyperons for complete amplitude analyses in reactions such as $KN \to \pi^+\pi^-\Lambda$, $\pi N \to K^+\pi^-\Lambda$, and others. The new generation of experiments with spin will advance not only the experimental hadron spectroscopy but also our theoretical understanding of hadron constituent structure, hadron wave function in the nonperturbative regime, and the mechanism of hadron production.

ACKNOWLEDGMENTS

We thank A. B. Wicklund for kindly providing us with numerical tables of Argonne results on $p_\uparrow p \to \Delta^{++}n$ experiment with polarized proton beam. This work was supported by Commissariat à l'Energie Atomique, Saclay, FCAR pour l'Aide et le Soutien a la Recherche du Gouvernement du Québec France and, in part, by Fonds Ministère de l'Education du Québec, Canada.

APPENDIX

Consider a binary reaction $A+B \to C+D$. The spin labels of scattering amplitudes correspond to spin states of each particle in its own rest frame. The spin labels depend on the choice of these rest frames which, in principle, could be chosen differently for each particle.

Helicity of a particle is the component of its spin along the particle's momentum in a given frame of reference. When the rest frame z axis has the direction of the particle momentum in the center-of-mass system of the reaction $A+B \to C+D$, we speak of helicity rest frame or s-channel helicity rest frame. The y axis is usually chosen in the direction of the normal to the scattering plane defined according to Basel convention by $\mathbf{P}_A \times \mathbf{P}_C$. For the purposes of this Appendix we will refer to this choice of y axis as the Argonne-CERN-Munich (ACM) convention. Recently Bourrely, Leader, and Soffer (BLS) argued[43] that the y axis of particles B and D should be opposite to the normal. Clockwise rotation about the common z axis by 180° rotates the ACM helicity frame to the BLS helicity frame, and vice versa.

A rotation about the helicity z axis by an angle α produces a phase change in the particle helicity state:

$$|\mathbf{p};\lambda\rangle \to e^{i\alpha\lambda}|\mathbf{p};\lambda\rangle \ . \tag{A1}$$

The helicity amplitudes in the ACM and BLS frames are related by a simple phase factor

$$(H_{\lambda_3\lambda_4,\lambda_1\lambda_2})_{\rm ACM} = \exp[i\pi(\lambda_4-\lambda_2)] \times (H_{\lambda_3\lambda_4,\lambda_1\lambda_2})_{\rm BLS} \ . \tag{A2}$$

Since $\alpha=\pi$, the inverse relation has the same phase factor. When the particles B and D are nucleons, the phase factor is simply $(-1)^n$ where $n=|\lambda_4-\lambda_2|$ is nucleon helicity flip.

In general, mixed helicity-transversity amplitudes $T_{\lambda_3\tau_4,\lambda_1\tau_2}$ are defined in terms of helicity amplitudes $H_{\lambda_3\lambda_4,\lambda_1\lambda_2}$ as follows:

$$T_{\lambda_3\tau_4,\lambda_1\tau_2} = \sum_{\lambda_2,\lambda_3} \mathcal{D}^{(S_4)*}_{\tau_4\lambda_4} \mathcal{D}^{(S_2)}_{\lambda_2\tau_2} \zeta H_{\lambda_3\lambda_4,\lambda_1\lambda_2} \ , \tag{A3}$$

where

$$\mathcal{D}^{(S)}_{\tau\lambda} = \exp\left[i\frac{\pi}{2}(\lambda-\tau)\right] d^S_{\tau\lambda}\left[\frac{\pi}{2}\right] \tag{A4}$$

are rotation matrices describing the transversity frame first defined by Kotanski.[55]

When the helicity amplitudes are defined in the ACM frame and the factor

$$\zeta = 1 \tag{A5}$$

then the quantization $+z$ axis in the transversity frame is along the Basel normal. When the helicity amplitudes are defined in the BLS frame and the factor ζ is

$$\zeta = \exp[i\pi(\lambda_4-\lambda_2)] \tag{A6}$$

then the BLS amplitudes are first rotated to the ACM frame and, upon the rotation (A4), we reach the same transversity frame.

To distinguish the two frames in the following discussion, we introduce a sign factor such that $\xi=-1$ and $\xi=+1$ for helicity amplitudes in the ACM and BLS frame, respectively. The sign factor merely reflects the fact that nucleon-helicity-flip amplitudes differ by a sign in the two frames.

In the case of a reaction such as $KN \to K\pi N$ we consider the dimeson state with definite spin J as the particle C. The results of explicit calculations for S- and P-wave amplitudes $T^J_{\lambda\tau_p,0\lambda_n}$ read

$$\frac{1}{\sqrt{2}}(S_0+i\xi S_1) = -\frac{i}{\sqrt{2}} T^{(0)}_{0\uparrow,0\downarrow} \ , \qquad \frac{1}{\sqrt{2}}(S_0-i\xi S_1) = +\frac{i}{\sqrt{2}} T^{(0)}_{0\downarrow,0\uparrow} \ , \tag{A7}$$

$$\frac{1}{\sqrt{2}}(L_0+i\xi L_1) = -\frac{i}{\sqrt{2}} T^{(1)}_{0\uparrow,0\downarrow} \ , \qquad \frac{1}{\sqrt{2}}(L_0-i\xi L_1) = +\frac{i}{\sqrt{2}} T_{0\downarrow,0\uparrow} \ , \tag{A8}$$

$$\frac{1}{\sqrt{2}}(U_0+i\xi U_1) = -iT^{(1)}_{+1\uparrow,0\downarrow} = +iT^{(1)}_{-1\uparrow,0\downarrow} \ , \qquad \frac{1}{\sqrt{2}}(U_0-i\xi U_1) = +iT^{(1)}_{+1\downarrow,0\uparrow} = -iT^{(1)}_{-1\downarrow,0\uparrow} \ , \tag{A9}$$

$$\frac{1}{\sqrt{2}}(N_0+i\xi N_1) = T^{(1)}_{+1\uparrow,0\uparrow} = T^{(1)}_{-1\uparrow,0\uparrow} \ , \qquad \frac{1}{\sqrt{2}}(N_0=i\xi N_1) = T^{(1)}_{+1\downarrow,0\downarrow} = T^{(1)}_{-1\downarrow,0\downarrow} \ . \tag{A10}$$

In this paper we work with the ACM frame. It is evident from Eqs. (A7)–(A10) that our transversity amplitudes $\bar{S},\bar{L},\bar{U},\bar{N}$ (S,L,U,N) defined in Eq. (2.18) correspond to spin "up" ("down") along the Basel normal.

As the consequence of parity conservation, the transversity amplitudes (A9) and (A10) do not distinguish between dimeson helicity states $\lambda=\pm1$. In the transversi-

ty frame, the production of dimeson states with helicities $\lambda=\pm1$ depends only on the transversities of the initial and final nucleons. Parity conservation also requires that

$$T^{(0)}_{0\uparrow,0\uparrow}=T^{(0)}_{0\downarrow,0\downarrow}=0,\quad T^{(1)}_{0\uparrow,0\uparrow}=T^{(1)}_{0\downarrow,0\downarrow}=0\ . \tag{A11}$$

The production of dimeson states with helicity $\lambda=0$ is forbidden by parity conservation when the initial and final nucleons have the same transversities.

It is also possible to define mixed amplitudes

$$F_{\lambda_3\tau_4,\lambda_1\lambda_2}=\sum_{\lambda_4}\mathcal{D}^{(S_4)}_{\tau_4\lambda_4}\xi H_{\lambda_3\lambda_3,\lambda_1\lambda_2} \tag{A12}$$

with only the recoil nucleon in transversity states. In this convention we then also have the following relations[41] for the amplitudes (5.18):

$$S=iF^{(0)}_{0\downarrow,0+},\quad \bar{S}=F^{(0)}_{0\uparrow,0+}\ , \tag{A13}$$

$$L=iF^{(1)}_{0\downarrow,0+},\quad \bar{L}=F^{(1)}_{0\uparrow,0+}\ , \tag{A14}$$

$$U=\frac{i}{\sqrt{2}}(F^{(1)}_{+1\downarrow,0+}-F^{(1)}_{-1\downarrow,0+})\ ,$$
$$\bar{U}=\frac{1}{\sqrt{2}}(F^{(1)}_{+1\uparrow,0+}-F^{(1)}_{-1\uparrow,0+})\ , \tag{A15}$$

$$N=\frac{i}{\sqrt{2}}(F^{(1)}_{+1\downarrow,0+}+F^{(1)}_{-1\downarrow,0+})\ ,$$
$$\bar{N}=\frac{1}{\sqrt{2}}(F^{(1)}_{+1\uparrow,0+}+F^{(1)}_{-1\uparrow,0+})\ . \tag{A16}$$

In our opinion, the nucleon transversity amplitudes (A7)–(A10) used in this paper are more suitable for physical interpretation of results of measurements on transversely polarized targets.

We note that in our earlier papers[7,10–13,80–82] we worked with ACM helicity amplitudes which we rotated to BLS frame before applying the Kotanski rotation (A4). In this case the $+z$ axis in the transversity frame is opposite to the normal and so is the direction labeled as spin "up."

---

*Permanent address: Dawson College and McGill University, Montreal, Quebec, Canada.
†Present address: GIXI Ingénierie et Informatique, Paris, France.
‡Present address: AEI Industries, Tokyo, Japan.
§Present address: Los Alamos Scientific Laboratory, Los Alamos, New Mexico.
**Present address: National Institute of Radiological Science, Chiba, Japan.

[1]M. Babou *et al.*, Nucl. Instrum. Methods **160**, 1 (1979).
[2]L. van Rossum *et al.*, in *High Energy Physics with Polarized Beams and Polarized Targets,* proceedings of the Third International Symposium, Argonne, 1978, edited by G. H. Thomas (AIP Conf. Proc. 51) (AIP, New York, 1979), p. 478.
[3]M. Svec *et al.*, in *High Energy Physics with Polarized Beams and Polarized Targets* (Ref. 2), p. 491.
[4]M. Fujisaki *et al.*, Phys. Lett. **80B**, 314 (1979).
[5]M. Fujisaki *et al.*, Nucl. Phys. **B152**, 232 (1979).
[6]M. Fujisaki *et al.*, Nucl. Phys. **B151**, 206 (1979).
[7]A. de Lesquen *et al.*, Phys. Rev. D **32**, 21 (1985).
[8]M. Svec, A. de Lesquen, and L. van Rossum, in *Intersections Between Particle and Nuclear Physics,* Luke Louise, 1986, edited by Donald F. Geesaman (AIP Conf. Proc. 150) (AIP, New York, 1986), p. 1198.
[9]M. Fujisaki *et al.*, Nuovo Cimento **99A**, 395 (1988).
[10]A. de Lesquen *et al.*, in *Low and Intermediate Energy Kaon-Nucleon Physics,* edited by E. Ferrari and G. Violini (Reidel, Dordrecht, 1981), p. 289.
[11]M. Svec *et al.*, in *Low and Intermediate Energy Kaon-Nucleon Physics* (Ref. 10), p. 305.
[12]A. Itano *et al.*, in *High Energy Physics with Polarized Beams and Targets,* edited by C. Joseph and J. Soffer (Birkhauser, Boston, Cambridge, MA, 1981), p. 560.
[13]M. Svec *et al.*, in *High Energy Physics with Polarized Beams and Targets* (Ref. 12), p. 566.
[14]A. de Lesquen *et al.*, Centre d'Études Nucléaires de Saclay Internal Report No. DPhPE 82-01, 1982 (unpublished).
[15]M. Svec, A. de Lesquen, and L. van Rossum (unpublished).
[16]H. Becker *et al.*, Nucl. Phys. **B150**, 301 (1979); **B151**, 46 (1979); V. Chabaud *et al.*, *ibid.* **B223**, 1 (1983).
[17]K. Rybicky and I. Sakrejda, Z. Phys. C **28**, 65 (1985); K. Rybicky, I. Sakrejda, J. Turnau, Acta Phys. Pol. **B17**, 317 (1986).
[18]L. Gorlich *et al.*, Nucl. Phys. **B174**, 16 (1980).
[19]V. Chabaud *et al.*, Nucl. Phys. **B178**, 401 (1981).
[20]V. D. Apokin *et al.*, in *Proceedings of the Seventh International Symposium on High Energy Spin Physics,* Protvino, USSR, 1986 (Institute of High Energy Physics, Serpukhov, 1986), Vol. 2, p. 65.
[21]A. B. Wicklund *et al.*, Phys. Rev. D **35**, 2670 (1987).
[22]R. L. Eisner *et al.*, Phys. Rev. D **20**, 596 (1979).
[23]A. B. Wicklund *et al.*, Phys. Rev. D **34**, 19 (1986); A. B. Wicklund, Data Tables, Report No. ANL-HEP-TR-86-21, 1986 (unpublished).
[24]J. P. Finley *et al.*, Phys. Rev. D **33**, 2528 (1985).
[25]Y. Terrien *et al.*, SATURNE II Experiment No. E-140, 1986.
[26]N. E. Davison *et al.*, TRIUMF Experiment No. E-372, 1986.
[27]J. E. Brau *et al.*, Phys. Rev. D **37**, 2379 (1988).
[28]S. Goldhaber *et al.*, Phys. Rev. Lett. **15**, 737 (1965); G. Bassompierre *et al.*, Nucl. Phys. **B16**, 125 (1970); D. Cords *et al.*, Phys. Rev D **4**, 1974 (1971); K. Buchner *et al.*, Nucl. Phys. **B45**, 333 (1972); A. Firestone *et al.*, Phys. Rev. D **5**, 2188 (1972); D. Cords *et al.*, Nucl. Phys. **B54**, 109 (1973); K. Hendricks *et al.*, *ibid.* **B112**, 189 (1976); D. Vignaud *et al.*, Nuovo Cimento **41A**, 29 (1977); M. G. Bowler *et al.*, Nucl. Phys. **B126**, 31 (1977).
[29]A. B. Wicklund *et al.*, Phys. Rev. D **17**, 1197 (1978).
[30]P. Estabrooks *et al.*, Nucl. Phys. **B133**, 490 (1978).
[31]W. Ochs, Nuovo Cimento **12A**, 724 (1972); P. Estabrooks and A. D. Martin, Phys. Lett. **41B**, 350 (1972); B. Hyams *et al.*, Nucl. Phys. **B64**, 134 (1973).
[32]*Proceedings of the Conference on $\pi\pi$ and $K\pi$ Interactions,* Argonne National Laboratory, 1969, edited by F. Loeffler and E. Malamud (Argonne National Laboratory, Argonne, 1969).
[33]*π-π Scattering—1973,* Tallahassee, edited by D. K. Williams (AIP Conf. Proc. 13) (AIP, New York, 1973).
[34]J. L. Peterson, Phys. Rep. **2C**, 155 (1971); B. R. Martin, D. Morgan, and G. Show, *Pion-Pion Interactions in Particle*

Physics (Academic, New York, 1976); J. L. Peterson, *The $\pi\pi$ Interaction* (CERN Yellow Report No. 77-04, Geneva, 1977); C. B. Lang, Fortsch. Phys. **26**, 509 (1980).

[35]W. Ochs, in *Nucleon-Nucleon Interactions,* proceedings of the Second International Conference on Nucleon-Nucleon Interactions, edited by H. Fearing, D. Measday, and A. Strathdee (AIP Conf. Proc. 41) (AIP, New York, 1978), p. 326.

[36]E. Byckling and K. Kajantie, *Particle Kinematics* (Wiley, New York, 1973).

[37]S. Humble, *Introduction to Particle Production of Hadrons* (Academic, New York, 1974).

[38]R. Saenger and W. Schmidt, Ann. Phys. (N.Y.) **54**, 307 (1969); D. B. Ion and C. Mihul, *ibid.* **83**, 41 (1975).

[39]R. J. Cashmore, *Phenomenology of Particles at High Energies,* 14th Scottish Universities' Summer School in Physics, 1973, edited by R. L. Crawford and R. Jennings (Academic, New York, 1974), p. 611.

[40]J. D. Kimel and J. F. Owens, Nucl. Phys. **B122**, 464 (1977).

[41]G. Lutz and K. Rybicky, Max Planck Institute, Munich, Internal Report No. MPI-PAE/Exp. EI.75, 1978 (unpublished).

[42]I. Sakrejda, Ph.D. thesis, Institute of Nuclear Physics, Cracow, 1984, Report No. 1262/PM.

[43]C. Bourrely, E. Leader, and J. Soffer, Phys. Rep. **59**, 95 (1980).

[44]M. N. Jones, *Spherical Harmonics and Tensors for Classical Field Theory* (Wiley, New York, 1985).

[45]R. L. Sekulin, Nucl. Phys. **B56**, 227 (1973).

[46]G. Grayer *et al.*, Nucl. Phys. **B75**, 189 (1974).

[47]M. G. Doncel *et al.*, Nucl. Phys. **38**, 477 (1972); M. G. Doncel *et al.*, Fortsch. Phys. **24**, 259 (1976).

[48]G. Grayer *et al.*, Nucl. Phys. **B50**, 29 (1972).

[49]S. U. Chung and T. L. Trueman, Phys. Rev. D **11**, 633 (1975).

[50]S. Meyers *et al.*, Phys. Rev. D **17**, 777 (1978).

[51]G. Alexander *et al.*, Nucl. Phys. **B157**, 425 (1979).

[52]Y. Alhassid and R. D. Levine, Phys. Rev. D **18**, 89 (1978); R. D. Levine, *The Maximum Entropy Formalism* (MIT, Cambridge, MA, 1979), p. 247.

[53]S. Dagan and Y. Dothan, Phys. Rev. D **26**, 248 (1982).

[54]P. La France and P. Winternitz, Phys. Rev. D **27**, 112 (1983).

[55]A. Kotanski, Acta Phys. Pol. **29**, 699 (1966); **30**, 629 (1966); **B1**, 45 (1970).

[56]G. Cohen-Tannoudji *et al.*, Ann. Phys. (N.Y.) **46**, 239 (1968).

[57]T. Niinikoski, in *High Energy Physics with Polarized Beams and Targets,* Argonne, 1976, edited by M. L. Marshak (AIP Conf. Proc. 35) (AIP, New York, 1977), p. 458; K. Guckelsberger and F. Udo, Nucl. Instrum. Methods **137**, 415 (1976).

[58]Ph. E. Gill, W. Murray, and M. H. Wright, *Practical Optimization* (Academic, New York, 1981).

[59]B. A. Murtagh and M. A. Saunders, MINOS 5.0 Users Guide, Systems Optimization Laboratory Report No. SOL 83-20, Stanford University, 1983 (unpublished).

[60]S. S. Rao, *Optimization and Application* (Wiley, New York, 1984), p. 723.

[61]W. T. Eadie *et al.*, *Statistical Methods in Experimental Physics* (North-Holland, Amsterdam, 1971), p. 159.

[62]R. Gilmore, *Catastrophe Theory for Scientists and Engineers* (Wiley, New York, 1981).

[63]J. M. T. Thompson and H. B. Stewart, *Nonlinear Dynamics and Chaos* (Wiley, New York, 1986).

[64]C. Evangelista *et al.*, Nucl. Phys. **B165**, 383 (1980).

[65]M. L. Goldberg and K. M. Watson, *Collision Theory* (Wiley, New York, 1964), p. 504.

[66]Byckling and Kajantie, *Particle Kinematics* (Ref. 36), pp. 115 and 257.

[67]W. Michael, Phys. Rev. D **7**, 1985 (1973); J. MacNaughton *et al.*, Nucl. Phys. **B108**, 75 (1976).

[68]A. Bialas and K. Zalewski, Nucl. Phys. **B6**, 449 (1968); **B6**, 465 (1968); **B6**, 478 (1968).

[69]H. Lipkin, Nucl. Phys. **B20**, 652 (1970); Phys. Rep. **8C**, 173 (1973).

[70]R. D. Field, in *Proceedings of the Brookhaven National Laboratory Workshop on Physics with Polarized Targets,* Upton, New York, 1974, edited by J. S. Russ (National Technical Information Service, Springfield, VA, 1975), p. 99.

[71]A. B. Wicklund, Argonne Report No. ANL-HEP-CP-75-73, 1975, p. 112 (unpublished).

[72]M. Zralek *et al.*, Phys. Rev. D **19**, 820 (1979).

[73]A. Donnachie and P. V. Landshoff, Phys. Lett. **95B**, 437 (1980).

[74]S. Fredrikson *et al.*, Phys. Rev. Lett. **51**, 2179 (1983).

[75]I. G. Aznauryan *et al.*, Phys. Lett. **126B**, 271 (1983).

[76]C. Lovelace, in *Proceedings of the Conference on $\pi\pi$ and $K\pi$ Interactions* (Ref. 32), p. 562.

[77]M. Yuta *et al.*, Phys. Rev. Lett. **26**, 1502 (1971).

[78]D. Cords *et al.*, Nucl. Phys. **B54**, 109 (1973); S. L. Baker *et al.*, *ibid.* **B99**, 211 (1975).

[79]J. J. Engelen *et al.*, Nucl. Phys. **B134**, 14 (1978).

[80]M. Svec, in *Proceedings of the XXII International Conference on High Energy Physics,* Leipzig, East Germany, 1984, edited by A. Meyer and E. Wieczorek (Akademie der Wissenschaften der DOR, Zeuthen, 1984).

[81]M. Svec, J. Phys. (Paris) Colloq. **46**, C2-281 (1985).

[82]M. Svec, in *Hadron Spectroscopy—1985,* College Park, Maryland, edited by S. Oneda (AIP Conf. Proc. 132) (AIP, New York, 1985), p. 68.

[83]C. Dover, in *Interactions Between Particle and Nuclear Physics* (Ref. 8), p. 272.

[84]G. P. Court, in *High Energy Spin Physics—1982,* Brookhaven National Laboratory, 1982, edited by G. M. Bunce (AIP Conf. Proc. 95) (AIP, New York, 1982), p. 464.

[85]R. Bernard *et al.*, Nucl. Instrum. Methods **249**, 176 (1986).

[86]T. Niinikoski, in *High Energy Spin Physics* (Ref. 84), p. 367.

[87]*Proceedings of the 4th International Workshop on Polarized Target Materials and Techniques,* Bad Honnef, West Germany, 1984, edited by W. Meyer (University of Bonn, Bonn, 1984); *Proceedings of the International Workshop on Polarized Sources and Targets,* Montana, Switzerland, 1986, edited by S. Jaccard and S. Mango [Helv. Phys. Acta **59**, No. 4 (1986)].

[88]D. Kleppner and T. J. Greytak, in *High Energy Spin Physics,* (Ref. 84), p. 546.

[89]R. R. Whitney, Research Program at Continuous Electron Beam Accelerator Facility, CEBAF report, 1986, Sec. 12.1 (unpublished).

[90]J. Kirkby *et al.*, Report No. CERN/PSCC 86-23, 1986 (unpublished).

[91]E. Vogt, Nucl. Phys. **A450**, 453c (1986); J. Domigo, *ibid.* **A450**, 473c (1986); G. T. Garvey, *ibid.* **A450**, 539c (1986).

[92]Canadian Kaon Factory, TRIUMF, 1985.

[93]*Physics and a Plan for a 45 GeV Facility* (Report No. LA-10720-MS, Los Alamos, 1986).

[94]*Proceedings of the International Conference on a European Hadron Facility,* Mainz, Germany, 1986, edited by T. Walcher [Nucl. Phys. **B279**, 2 (1987)].

[95]*International Workshop on Hadron Facility Technology,* Los Alamos, 1987, edited by H. A. Thiessen (LANL Report No.

LA-11130-C, Los Alamos, 1987).
[96]Japanese Hadron Facility (Ref. 95), p. 67.
[97]Moscow Meson Facility, Intense Hadron Facility Users' Group Newsletter No. 2 (TRIUMF, Vancouver, 1988).
[98]Y. Onel, and A. Penzo, Surv. High Energy Phys. **5**, 1 (1985).
[99]Y. Onel, A. Penzo, and R. Rossmanith, in *Workshop on Fermilab Low Energy Antiproton Facility* (Fermilab, Batavia, 1986); Y. Onel, A. Penzo, and R. Rossmanith, in *Intersections Between Particle and Nuclear Physics* (Ref. 8), p. 1229.